A projection hybrid high order finite volume/finite element method for incompressible turbulent flows

S. Busto[a], J.L. Ferrín[a,b], E. F. Toro[c], M.E. Vázquez-Cendón[a,b,*]

[a] *Departamento de Matemática Aplicada, Universidade de Santiago de Compostela, Facultad de Matemáticas. ES-15782 Santiago de Compostela, Spain*
[b] *ITMATI, Campus Sur. ES-15782 Santiago de Compostela, Spain*
[c] *Laboratory of Applied Mathematics, DICAM, University of Trento. IT-38100 Trento, Italy*

Abstract

In this paper the projection hybrid FV/FE method presented in [1] is extended to account for species transport equations. Furthermore, turbulent regimes are also considered thanks to the $k-\varepsilon$ model. Regarding the transport diffusion stage new schemes of high order of accuracy are developed. The CVC Kolgan-type scheme and ADER methodology are extended to 3D. The latter is modified in order to profit from the dual mesh employed by the projection algorithm and the derivatives involved in the diffusion term are discretized using a Galerkin approach. The accuracy and stability analysis of the new method are carried out for the advection-diffusion-reaction equation. Within the projection stage the pressure correction is computed by a piecewise linear finite element method. Numerical results are presented, aimed at verifying the formal order of accuracy of the scheme and to assess the performance of the method on several realistic test problems.

Keywords: incompressible flows, $k-\varepsilon$ model, species transport, projection method, finite volume method, LADER, finite element method.

*Corresponding author

Email addresses: saray.busto@usc.es (S. Busto), joseluis.ferrin@usc.es (J.L. Ferrín), eleuterio.toro@unitn.it (E. F. Toro), elena.vazquez.cendon@usc.es (M.E. Vázquez-Cendón)

1. Introduction

Finite volume methods combined with approximate Riemann solvers have been successfully developed for different kinds of flows in the 1980's (see, [2] and the references therein). Focusing on the incompressible case, pressure results in a Lagrange multiplier that adapts itself to ensure that the velocity satisfies the incompressibility condition. In order to handle this situation, the typical explicit stage of finite volume methods has to be complemented with the so-called projection stage where a pressure correction is computed in order to get a divergence-free velocity. Many papers exist in the literature devoted to introduce and analyse projection finite volume methods for incompressible Navier-Stokes equations (see, for instance, [3] or [4]). In order to get stability, staggered grids have been used to discretize velocity and pressure. While this can be done straightforwardly in the context of structured meshes, the adaptation to unstructured meshes is more challenging (see [5], [6], [7], [8], [9], [10]).

On the other hand, projection methods have been also used in combination with finite element discretizations (see [11]). Within this approach, the divergence-free condition for the velocity is replaced by an equation prescribing the divergence of the linear momentum density which is a conservative variable.

The scope of this paper is to extend the hybrid FV/FE projection method introduced in [1] for both laminar and turbulent flows considering also transport of species. Furthermore, new methods to increase the accuracy of the methodology are developed.

Starting from a 3D tetrahedral finite element mesh of the computational domain, the equation of the transport-diffusion stage is discretized by a finite volume method associated with a dual finite volume mesh where the nodes of the volumes are the barycentre of the faces of the initial tetrahedra. These volumes, which allow us for an easy implementation of flux boundary conditions, have already been used, among others, for the 2D shallow water equation (see [5]), for solving conservative and non conservative systems in 2D and 3D (see [12] and [13]) and for DG schemes employed to solve compressible Navier-Stokes equations (see [14]). For time discretization we use the explicit Euler scheme. The convective term is upwinded using the Rusanov scheme (see [2] and [15]). Concerning the projection stage, the pressure correction is computed by continuous piecewise linear finite elements associated with the initial tetrahedral mesh. The use of the above "staggered"

meshes together with a simple specific way of passing the information from the transport-diffusion stage to the projection one and vice versa leads to a stable scheme. The former is done by redefining the conservative variable (i.e. the momentum density) constant per tetrahedron. Conversely, the finite element pressure correction is redefined to constant values on the faces of the finite volumes and then used in the transport-diffusion stage.

The coupling of Navier-Stokes equations and the turbulence model introduces turbulent viscosity which is typically computed by solving an additional pair of advection-diffusion-reaction equations, that is equations for the turbulent kinetic energy and the dissipation rate. One issue here is the time dependency of the viscous terms. This requires the use of methods that are at least second-order accurate in space and time for all terms involved (see [16] and [17]).

For advection equations, several approaches for constructing high-order methods have been put forward. A classical example is the Lax-Wendroff scheme (see [18] and [19]). This scheme is linear in the sense of Godunov and thus oscillatory, according to Godunov's theorem, [20]. A major step forward in this direction was the work of Kolgan [21], who introduced, for the first time, a numerical scheme that circumvents Godunov's theorem, via the construction of a non-linear scheme using non-linear reconstructions (see [22]). Following these works, a new Kolgan-type method has been presented for the shallow water equations in [23]. In what follows, we will refer to this scheme as the CVC Kolgan-type scheme.

In the present paper, the CVC Kolgan-type scheme is analysed and implemented at the transport-diffusion stage for the convective terms of the considered conservation laws: momentum conservation, transport equations and k-ε model. The obtained scheme, second order in space and first order in time is combined with a Galerkin approach of the gradients involved in the viscous term. An alternative option will be the decomposition of the diffusion term into its orthogonal and non-orthogonal parts as introduced in [1].

More advanced non-linear methods for advection dominated problems have appeared in the literature since the introduction of Kolgan scheme. Some of them are: Total Variation Diminishing Methods (TVD), Flux Limiter Methods, MUSCL-Hancock, semi-discrete ENO or WENO (see, for instance, [24], [25], [26], [24], [27], [28], [29] and [30]). Comprehensive reviews are found in [2] and [31], for example. Focusing on high order in time and space methodologies, we highlight the ADER approach, first put forward in

[32]. It is also a fully discrete approach that relies on non-linear reconstructions and the solution of the generalised Riemann problem, to any order of accuracy. The resulting schemes are arbitrarily accurate in both space and time in the sense that they have no theoretical accuracy barrier. An introduction to ADER schemes is found in Chapters 19 and 20 of [2]. Further developments and applications are found, for example, in [33], [34], [35], [36], [37], [38], [39], [40], [41], [42], [43], [44], [45], [46], [47], [48], [49].

In [50] an extension of ADER methodology to solve the advection-diffusion-reaction equation, admitting space and time dependent diffusion coefficients was introduced. The present work includes a modification of this scheme, the Local ADER method (LADER), which profits from the dual mesh. Moreover, an ENO-based reconstruction is considered in order to prevent spurious oscillations.

To asses the performance of the methodology different manufactured solution tests are introduced and the numerical results obtained with the developed computer code are shown. Furthermore, several classical test problems from fluid mechanics are presented and some results are compared with experimental data (see [17] and [1]).

The paper is organized as follows. In Section 2 the mathematical model for incompressible flows is recalled. Then, the RANS $k-\varepsilon$ model for the turbulence and the species transport equations are described. In Section 3 the numerical discretization is detailed. Special attention is paid to the description of the finite volume algorithm. Aiming to achieve a high order scheme, two different methodologies for the flux terms are developed: the CVC Kolgan-type method, second order in space and first order in time, and the LADER methodology, second order in space and time. The needed modifications on the approximation of remaining terms of the equations to achieve a high order scheme are also presented and a Galerkin approach to compute the diffusion terms is introduced. Finally, in Section 4 some of the numerical results obtained with the developed code are shown. On the one hand, the order of convergence of the method is analysed using the method of manufactured solutions. On the other hand, several classical test problems are analysed. The appendix includes the theoretical analysis of the LADER numerical method applied to the one-dimensional advection-diffusion-reaction equation.

2. Governing equations

In this section, the system of equations to be solved is introduced. The model for incompressible newtonian fluids, recalled in [1], is extended considering a turbulent regime and taking into account the transport of species.

2.1. Mass conservation and momentum equations

The incompressible Navier-Stokes equations reduce to the mass conservation equation and the momentum equation. Hence, the system of equations written in conservative variables reads

$$\mathrm{div}\mathbf{w_u} = 0, \tag{1}$$

$$\frac{\partial \mathbf{w_u}}{\partial t} + \mathrm{div}\mathcal{F}^{\mathbf{w_u}}(\mathbf{w_u}) + \nabla\pi - \mathrm{div}(\tau) = \mathbf{f_u}. \tag{2}$$

Standard notation is used:

- ρ is the density (kg/m^3),
- $p = \pi + \overline{\pi}$ is the pressure (N/m^2),
  - $\overline{\pi}$ is the mean pressure,
  - π is the pressure perturbation,
- $\mathbf{u} = (u_1, u_2, u_3)^t$ is the velocity vector (m/s),
- $\mathbf{w_u} := \rho\mathbf{u}$ is the vector of the conservative variables related to the velocity (kg/s m^2),
- $\mathcal{F}^{\mathbf{w_u}}$ is the flux tensor:

$$\mathcal{F}_i^{\mathbf{w_u}}(\mathbf{w_u}) = \frac{1}{\rho}\mathbf{w}_i\mathbf{w_u} = u_i\mathbf{w_u},\ i = 1, 2, 3,$$

- τ is the viscous part of the Cauchy stress tensor,
- $\mathbf{f_u}$ is a generic source term used for the manufactured test problems.

2.2. Turbulence model

Special care for the viscous part of Cauchy stress tensor, τ, is required for turbulent regimes. In order to avoid the high computational cost of a direct simulation of the turbulence, the $k-\varepsilon$ standard model is used (see [51] and [52]). The Reynolds-averaged viscous stress tensor is given by

$$\tau = \tau_{\mathbf{u}} + \tau^{\mathbf{R}}. \tag{3}$$

Denoting μ the laminar viscosity (kg/(m s)), the averaged stress tensor, $\tau_{\mathbf{u}}$, reads

$$\tau_{\mathbf{u}} = \mu \left(\nabla \mathbf{u} + \nabla \mathbf{u}^T \right). \tag{4}$$

The fluctuation, $\tau^{\mathbf{R}}$, called the Reynolds tensor, is given by

$$\tau^{\mathbf{R}} = \mu_t \left(\nabla \mathbf{u} + \nabla \mathbf{u}^T \right) - \frac{2}{3} \rho k \mathbf{I}. \tag{5}$$

To obtain the turbulent viscosity,

$$\mu_t = \rho C_\mu \frac{k^2}{\varepsilon}, \tag{6}$$

two new variables are introduced: the turbulent kinetic energy, k (J/kg), and the energy dissipation rate, ε (J/(kg s)). They are computed from a new pair of partial differential equations, namely,

$$\frac{\partial w_k}{\partial t} + \mathrm{div} \mathcal{F}^{w_k} \left(w_k, \mathbf{u} \right) - \mathrm{div} \left[\left(\mu + \frac{\mu_t}{\sigma_k} \right) \nabla \left(\frac{w_k}{\rho} \right) \right] + w_\varepsilon = G_k + f_k, \tag{7}$$

$$\frac{\partial w_\varepsilon}{\partial t} + \mathrm{div} \mathcal{F}^{w_\varepsilon} \left(w_\varepsilon, \mathbf{u} \right) - \mathrm{div} \left[\left(\mu + \frac{\mu_t}{\sigma_\varepsilon} \right) \nabla \left(\frac{w_\varepsilon}{\rho} \right) \right] + C_{2\varepsilon} \frac{w_\varepsilon^2}{w_k} = C_{1\varepsilon} \frac{w_\varepsilon}{w_k} G_k + f_\varepsilon, \tag{8}$$

where

- w_k (J), w_ε (J/s) are the conservative variables corresponding to k and ε, that is
$$w_k := \rho k, \quad w_\varepsilon := \rho \varepsilon,$$
- $\mathcal{F}^{w_k}$, $\mathcal{F}^{w_\varepsilon}$ are the fluxes related to the turbulence variables,
$$\mathcal{F}_i^{w_k} \left(w_k, \mathbf{u} \right) = u_i w_k, \quad \mathcal{F}_i^{w_\varepsilon} \left(w_\varepsilon, \mathbf{u} \right) = u_i w_\varepsilon,$$

- G_k is the term of kinetic energy production, due to the mean velocity gradients, of the Reynolds stress tensor,

$$G_k = \frac{\mu_t}{2}\left[\sum_{i=1}^{3}\sum_{j=1}^{3}\left(\frac{\partial u_i}{\partial x_j}+\frac{\partial u_j}{\partial x_i}\right)\right]^2, \tag{9}$$

- f_k, f_ε are the source terms related to manufactured solutions for analytical tests; they have zero value in physical problems,
- $\sigma_k = 1.0$, $\sigma_\varepsilon = 1.3$ are the turbulent Prandtl numbers,
- $C_\mu = 0.09$, $C_{1\varepsilon} = 1.44$, $C_{2\varepsilon} = 1.92$ are the closure coefficients of the model whose values were taken from the literature.

2.3. Species transport

The equations of transport of species are also included in the system to be solved:

$$\frac{\partial \mathbf{w_y}}{\partial t} + \mathrm{div}\mathcal{F}^{\mathbf{w_y}}\left(\mathbf{w_y}, \mathbf{u}\right) - \mathrm{div}\left[\left(\rho\mathcal{D} + \frac{\mu_t}{Sc_t}\right)\nabla\left(\frac{1}{\rho}\mathbf{w_y}\right)\right] = \mathbf{f_y}, \tag{10}$$

with

- $\mathbf{y} = (\mathrm{y}_1, \ldots, \mathrm{y}_{N_e})^T$ the mass fraction vector of the species to be considered. y_i corresponds to species i and N_e is the total number of species to be considered,
- $\mathbf{w_y} := \rho\mathbf{y}$ the conservative variable vector related to the mass fraction vector,
- $\mathcal{F}^{\mathbf{w_y}}$ the flux,

$$\mathcal{F}_i^{\mathbf{w_y}}\left(\mathbf{w_y}, \mathbf{u}\right) = u_i\mathbf{w_y}$$

- $\mathcal{D}$ the mass diffusivity coefficient (m^2/s),
- $Sc_t = 0.7$ the turbulent Schmidt number,
- $\mathbf{f_y}$ the source term for manufactured test problems.

2.4. Complete system

The complete system of equations to be solved is

$$\mathrm{div}\mathbf{w_u} = 0, \quad (11)$$

$$\frac{\partial \mathbf{w_u}}{\partial t} + \mathrm{div}\mathcal{F}^{\mathbf{w_u}}(\mathbf{w_u}) + \nabla\pi - \mathrm{div}(\tau) = \mathbf{f_u}, \quad (12)$$

$$\frac{\partial w_k}{\partial t} + \mathrm{div}\mathcal{F}^{w_k}(w_k, \mathbf{u}) - \mathrm{div}\left[\left(\mu + \frac{\mu_t}{\sigma_k}\right)\nabla\left(\frac{w_k}{\rho}\right)\right] + w_\varepsilon = G_k + f_k, \quad (13)$$

$$\frac{\partial w_\varepsilon}{\partial t} + \mathrm{div}\mathcal{F}^{w_\varepsilon}(w_\varepsilon, \mathbf{u}) - \mathrm{div}\left[\left(\mu + \frac{\mu_t}{\sigma_\varepsilon}\right)\nabla\left(\frac{w_\varepsilon}{\rho}\right)\right] + C_{2\varepsilon}\frac{w_\varepsilon^2}{w_k} = C_{1\varepsilon}\frac{w_\varepsilon}{w_k}G_k + f_\varepsilon, \quad (14)$$

$$\frac{\partial \mathbf{w_y}}{\partial t} + \mathrm{div}\mathcal{F}^{\mathbf{w_y}}(\mathbf{w_y}, \mathbf{u}) - \mathrm{div}\left[\left(\rho\mathcal{D} + \frac{\mu_t}{Sc_t}\right)\nabla\left(\frac{1}{\rho}\mathbf{w_y}\right)\right] = \mathbf{f_y}. \quad (15)$$

Moreover, the vector of the conservative variables is $\mathbf{w} = (\mathbf{w_u}, \widehat{\mathbf{w}})^T$, with $\widehat{\mathbf{w}}$ the vector of the conservative variables related with turbulence, and species, i.e., $\widehat{\mathbf{w}} = (w_k, w_\varepsilon, \mathbf{w_y})^T$. The flux tensor of the complete system has three components:

$$\mathcal{F} = (\mathcal{F}_1|\mathcal{F}_2|\mathcal{F}_3)_{(3+2+N_e)\times 3}, \quad \mathcal{F}_i(\mathbf{w}) = \frac{w_i}{\rho}\mathbf{w}, \quad i = 1, 2, 3. \quad (16)$$

3. Numerical discretization

The numerical discretization of the complete system is performed by extending the projection method first put forward in [1]. The developed numerical method solves, at each time step, equations (12)-(15) with a finite volume method (FVM) and, so, an approximation of $\mathbf{w}$ is obtained. The next step is applying projection to system (11)-(12). The pressure correction is provided by a piecewise linear finite element method (FEM). In the post-projection step, an approximation of $\mathbf{w_u}$ verifying the divergence condition, (11), is obtained. Furthermore, the production terms of the turbulence equations are also computed in this step to account for the corrected velocities. The reaction terms are treated via a semi-implicit method.

We start by considering a two-stage in time discretization scheme: in order to get the solution at time t^{n+1}, we use the previously obtained approximations $\mathbf{W}^n$ of the conservative variables $\mathbf{w}(x, y, z, t^n)$, $\mathbf{U}^n$ of the velocity $\mathbf{u}(x, y, z, t^n)$ and π^n of the pressure perturbation $\pi(x, y, z, t^n)$, and compute $\mathbf{W}^{n+1}$ and π^{n+1} from the following system of equations:

$$\frac{1}{\Delta t}\left(\widetilde{\mathbf{W}}_{\mathbf{u}}^{n+1} - \mathbf{W}_{\mathbf{u}}^n\right) + \mathrm{div}\mathcal{F}^{\mathbf{w_u}}(\mathbf{W}_{\mathbf{u}}^n) + \nabla\pi^n - \mathrm{div}(\tau^n) = \mathbf{f}_{\mathbf{u}}^n, \quad (17)$$

$$\frac{1}{\Delta t}\left(\mathbf{W}_{\mathbf{u}}^{n+1}-\widetilde{\mathbf{W}}_{\mathbf{u}}^{n+1}\right)+\nabla(\pi^{n+1}-\pi^{n})=0, \quad (18)$$

$$\mathrm{div}\mathbf{W}_{\mathbf{u}}^{n+1}=0, \quad (19)$$

$$\frac{1}{\Delta t}\left(\widetilde{W}_{k}^{n+1}-W_{k}^{n}\right)+\mathrm{div}\mathcal{F}^{w_k}\left(W_{k}^{n},\mathbf{U}^{n}\right)-\mathrm{div}\left[\left(\mu+\frac{\mu_t}{\sigma_k}\right)\nabla\frac{W_{k}^{n}}{\rho}\right]=0, \quad (20)$$

$$\frac{1}{\Delta t}\left(W_{k}^{n+1}-\widetilde{W}_{k}^{n+1}\right)+W_{\varepsilon}^{n}-G_{k}^{n+1}=f_{k}^{n}, \quad (21)$$

$$\frac{1}{\Delta t}\left(\widetilde{W}_{\varepsilon}^{n+1}-W_{\varepsilon}^{n}\right)+\mathrm{div}\mathcal{F}^{w_\varepsilon}\left(W_{\varepsilon}^{n},\mathbf{U}^{n}\right)-\mathrm{div}\left[\left(\mu+\frac{\mu_t^n}{\sigma_\varepsilon}\right)\nabla\frac{W_{\varepsilon}^{n}}{\rho}\right]=0, \quad (22)$$

$$\frac{1}{\Delta t}\left(W_{\varepsilon}^{n+1}-\widetilde{W}_{\varepsilon}^{n+1}\right)+C_{2\varepsilon}\frac{W_{\varepsilon}^{n+1}W_{\varepsilon}^{n}}{W_{k}^{n}}-C_{1\varepsilon}\frac{W_{\varepsilon}^{n}}{W_{k}^{n}}G_{k}^{n+1}=f_{\varepsilon}^{n}, \quad (23)$$

$$\frac{1}{\Delta t}\left(\widetilde{\mathbf{W}}_{\mathbf{y}}^{n+1}-\mathbf{W}_{\mathbf{y}}^{n}\right)+\mathrm{div}\mathcal{F}^{\mathbf{w_y}}\left(\mathbf{W}_{\mathbf{y}}^{n},\mathbf{U}^{n}\right)-\mathrm{div}\left[\left(\rho\mathcal{D}+\frac{\mu_t^n}{Sc_t}\right)\nabla\left(\frac{1}{\rho}\mathbf{W}_{\mathbf{y}}^{n}\right)\right]=0, \quad (24)$$

$$\frac{1}{\Delta t}\left(\mathbf{W}_{\mathbf{y}}^{n+1}-\widetilde{\mathbf{W}}_{\mathbf{y}}^{n+1}\right)=\mathbf{f}_{\mathbf{y}}^{n}. \quad (25)$$

Concerning the discretization of mass conservation and momentum equations, by adding equations (17)-(18), we easily see that the scheme is actually implicit for the pressure term. However, the writing above shows that the pressure and the velocity can be solved in three uncoupled stages. The first of them corresponds to equation (17) and will be called the transport-diffusion stage; it is explicit and allows us to compute the intermediate approximation of the conservative variables $\widetilde{\mathbf{W}}_{\mathbf{u}}^{n+1}$ (we notice that, in general, this approximation does not satisfy the divergence condition (19)). The second one, to be called the projection stage, is implicit; it consists of solving the coupled equations (18) and (19) with a finite element method to obtain the pressure correction $\delta^{n+1}:=\pi^{n+1}-\pi^{n}$. The last one is the post-projection stage; the intermediate approximation for the velocity conservative variables is updated with the pressure correction providing the final approximations $\mathbf{W}_{\mathbf{u}}^{n+1}$ and π^{n+1} (see [1] for further details).

As a novelty in this paper, for the remaining conservation laws the approximation of the conservative variables is obtained in two steps. At the transport-diffusion stage we compute an approximation of the conservative variables, $\widetilde{W}_{k}^{n+1}$, $\widetilde{W}_{\varepsilon}^{n+1}$ and $\widetilde{\mathbf{W}}_{\mathbf{y}}^{n+1}$, taking into account the corresponding flux and diffusion terms. Let us remark that at this stage the update of the approximations involves all the neighbouring nodes of the finite volume C_i.

On the other hand, the discretization of the source terms related to manufactured solutions or other production terms in equations (21), (23) and (25) involves pointwise evaluations at the cell C_i which will be computed at the post-projection stage. Furthermore, the production terms of the turbulence equations are computed taking into account the updated velocities and the reaction terms are treated via a semi-implicit method. As a result, we obtain the updated conservative variables $\widetilde{W}_k^{n+1}$, $\widetilde{W}_\varepsilon^{n+1}$ and $\widetilde{\mathbf{W}}_{\mathbf{y}}^{n+1}$.

Summarizing, the overall method consists of:

- *Transport-diffusion stage:* equations (17), (20), (22) and (24) are solved by a FVM.
- *Projection stage:* the pressure correction $\delta^{n+1} := \pi^{n+1} - \pi^n$ is obtained by solving equations (18) and (19) with a FEM.
- *Post-projection stage:* the $\widetilde{\mathbf{W}}_{\mathbf{u}}^{n+1}$ computed at the first stage is updated by using δ^{n+1} in order to obtain another approximation $\mathbf{W}_{\mathbf{u}}^{n+1}$, satisfying the divergence condition (19). Next, the turbulence and species variables are updated from equations (21), (23) and (25), respectively.

3.1. A dual finite volume mesh

For the space discretization we consider a 3D unstructured tetrahedral finite element mesh $\{T_k,\, i = 1, \ldots, nel\}$. From this mesh we build a *dual finite volume mesh* as introduced in [1] and [5]. The nodes, to be denoted by $\{N_i,\, i = 1, \ldots, nvol\}$, are the barycenters of the faces of the initial tetrahedra. In Figure 1 node N_i is the barycenter of the face defined by vertices V_1, V_2 and V_3 (see Figure 1). This is why we will call this finite volume of *face-type*.

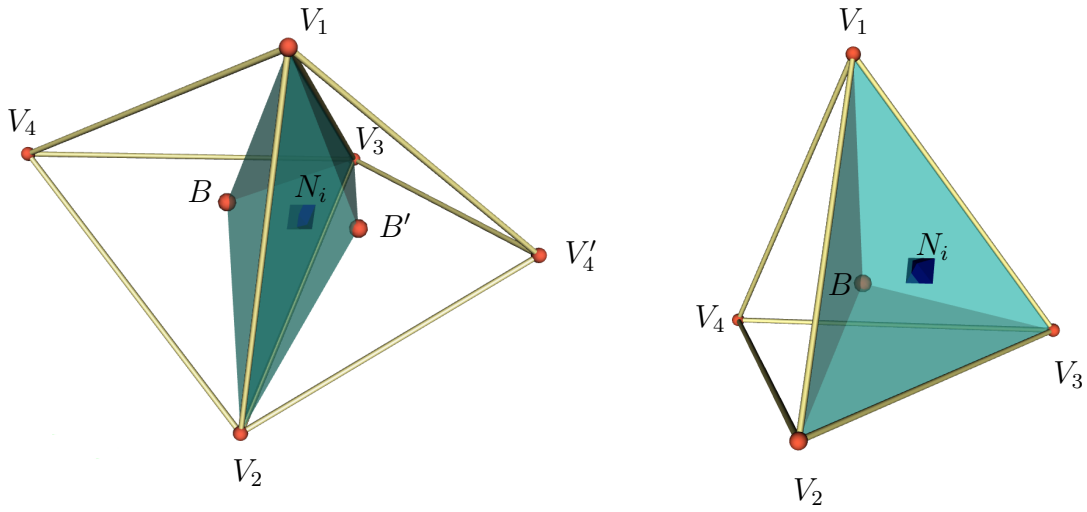

Figure 1: Interior (left) and boundary (right) finite volumes of the face-type.

The notation employed is as follows:

- Each interior node N_i has as neighboring nodes the set $\mathcal{K}_i$ consisting of the barycentres of the faces of the two tetrahedra of the initial mesh to which it belongs.
- The face Γ_{ij} is the interface between cells C_i and C_j. N_{ij} is the barycentre of the face.
- The boundary of C_i is denoted by $\Gamma_i = \bigcup_{N_j \in \mathcal{K}_i} \Gamma_{ij}$.
- Finally, $\widetilde{\boldsymbol{\eta}}_{ij}$ represents the outward unit normal vector to Γ_{ij}. We define $\boldsymbol{\eta_{ij}} := \widetilde{\boldsymbol{\eta}}_{\boldsymbol{ij}} ||\boldsymbol{\eta_{ij}}||$, where, $||\boldsymbol{\eta_{ij}}|| := \text{Area}(\Gamma_{ij})$.

3.2. Finite volume discretization

The discrete approximation of the conservative variables is taken to be constant per finite volume, as it represents an integral average. By integrating (17), (20), (22) and (24), on C_i and applying the Gauss Theorem, we get

$$\frac{1}{\Delta t}\left(\widetilde{\mathbf{W}}_{\mathbf{u},i}^{n+1} - \mathbf{W}_{\mathbf{u},\,i}^{n}\right) + \frac{1}{|C_i|}\int_{\Gamma_i} \mathcal{F}^{\mathbf{w_u}}\left(\mathbf{W}_{\mathbf{u}}^{n}\right)\tilde{\boldsymbol{\eta}}_i \mathrm{dS} + \frac{1}{|C_i|}\int_{C_i} \nabla \pi^n \mathrm{dV} - \frac{1}{|C_i|}\int_{\Gamma_i} \left(\tau^n\right)\tilde{\boldsymbol{\eta}}_i \mathrm{dS} = \frac{1}{|C_i|}\int_{C_i} \mathbf{f}_{\mathbf{u}}^{n} \mathrm{dV}, \tag{26}$$

$$\frac{1}{\Delta t}\left(\widetilde{W}_{k,i}^{n+1}-W_{k,i}^{n}\right)+\frac{1}{|C_i|}\int_{\Gamma_i}\mathcal{F}^{w_k}\left(W_k^n,\mathbf{U}^n\right)\tilde{\boldsymbol{\eta}}_i\mathrm{dS}-\frac{1}{|C_i|}\int_{\Gamma_i}\left[\left(\mu+\frac{\mu_t^n}{\sigma_k}\right)\nabla\frac{W_k^n}{\rho}\right]\tilde{\boldsymbol{\eta}}_i\mathrm{dS}=0, \tag{27}$$

$$\frac{1}{\Delta t}\left(\widetilde{W}_{\varepsilon,i}^{n+1}-W_{\varepsilon,i}^{n}\right)+\frac{1}{|C_i|}\int_{\Gamma_i}\mathcal{F}^{w_\varepsilon}\left(W_\varepsilon^n,\mathbf{U}^n\right)\tilde{\boldsymbol{\eta}}_i\mathrm{dS}-\frac{1}{|C_i|}\int_{\Gamma_i}\left[\left(\mu+\frac{\mu_t^n}{\sigma_\varepsilon}\right)\nabla\frac{W_\varepsilon^n}{\rho}\right]\tilde{\boldsymbol{\eta}}_i\mathrm{dS}=0, \tag{28}$$

$$\frac{1}{\Delta t}\left(\widetilde{\mathbf{W}}_{\mathbf{y},i}^{n+1}-\mathbf{W}_{\mathbf{y},i}^{n}\right)+\frac{1}{|C_i|}\int_{\Gamma_i}\mathcal{F}^{\mathbf{w_y}}\left(\mathbf{W}_{\mathbf{y}}^n,\mathbf{U}^n\right)\tilde{\boldsymbol{\eta}}_i\mathrm{dS}-\frac{1}{|C_i|}\int_{\Gamma_i}\left[\left(\rho\mathcal{D}+\frac{\mu_t^n}{Sc_t}\right)\nabla\left(\frac{1}{\rho}\mathbf{W}_{\mathbf{y}}^n\right)\right]\tilde{\boldsymbol{\eta}}_i\mathrm{dS}=0, \tag{29}$$

where $|C_i|$ denotes the volume of C_i and $\widetilde{\boldsymbol{\eta}}_i$ is the outward unit normal of Γ_i at each point. Within the following sections we will detail how to approximate the former integrals.

3.3. Numerical flux

We define the global normal flux on Γ_i as $\mathcal{Z}(\mathbf{W}^n,\tilde{\boldsymbol{\eta}}_i) := \mathcal{F}(\mathbf{W}^n)\tilde{\boldsymbol{\eta}}_i$. Thanks to the shape of the convective terms in equations (26)-(29) their integrals can be computed globally. We first split Γ_i into the cell interfaces Γ_{ij}, namely

$$\int_{\Gamma_i}\mathcal{F}(\mathbf{W}^n)\widetilde{\boldsymbol{\eta}}_i\,\mathrm{dS}=\sum_{N_j\in\mathcal{K}_i}\int_{\Gamma_{ij}}\mathcal{Z}(\mathbf{W}^n,\tilde{\boldsymbol{\eta}}_{ij})\,\mathrm{dS}. \tag{30}$$

Then, in order to obtain a stable discretization, the integral on Γ_{ij} is approximated by an upwind scheme using a numerical flux function ϕ:

$$\int_{\Gamma_{ij}}\mathcal{Z}(\mathbf{W}^n,\tilde{\boldsymbol{\eta}}_{ij})\mathrm{dS}\approx\phi\left(\mathbf{W}_i^n,\mathbf{W}_j^n,\boldsymbol{\eta}_{ij}\right). \tag{31}$$

The expression of ϕ depends on the upwind scheme. In this paper, we consider the Rusanov scheme (see [53]):

$$\begin{aligned}\phi\left(\mathbf{W}_i^n,\mathbf{W}_j^n,\boldsymbol{\eta}_{ij}\right)=&\frac{1}{2}(\mathcal{Z}(\mathbf{W}_i^n,\boldsymbol{\eta}_{ij})+\mathcal{Z}(\mathbf{W}_j^n,\boldsymbol{\eta}_{ij}))\\&-\frac{1}{2}\alpha_{RS}(\mathbf{W}_i^n,\mathbf{W}_j^n,\boldsymbol{\eta}_{ij})\left(\mathbf{W}_j^n-\mathbf{W}_i^n\right),\end{aligned} \tag{32}$$

where the coefficient α_{RS} can be computed in a coupled way for all the equations, so that, it is defined by

$$\alpha_{RS}(\mathbf{W}_i^n,\mathbf{W}_j^n,\boldsymbol{\eta}_{ij}):=\max\left\{2\left|\mathbf{U}_i^n\cdot\boldsymbol{\eta}_{ij}\right|,2\left|\mathbf{U}_j^n\cdot\boldsymbol{\eta}_{ij}\right|\right\} \tag{33}$$

or, we can consider

$$\alpha_{RS}^{\mathbf{w_u}}(\mathbf{W}_i^n, \mathbf{W}_j^n, \boldsymbol{\eta}_{ij}) := \max\left\{2\left|\mathbf{U}_i \cdot \boldsymbol{\eta}_{ij}\right|, 2\left|\mathbf{U}_j \cdot \boldsymbol{\eta}_{ij}\right|\right\} \tag{34}$$

for the momentum equation and

$$\hat{\alpha}_{RS}(\mathbf{W}_i^n, \mathbf{W}_j^n, \boldsymbol{\eta}_{ij}) := \max\left\{\left|\mathbf{U}_i \cdot \boldsymbol{\eta}_{ij}\right|, \left|\mathbf{U}_j \cdot \boldsymbol{\eta}_{ij}\right|\right\} \tag{35}$$

for the remaining equations.

Directly using the value obtained for the conservative variables at each node at the previous time step, Rusanov scheme is first order in space and time. Two different methodologies will be introduced in order to obtain second order schemes: the Kolgan-type scheme and the LADER scheme.

3.3.1. Kolgan-type scheme

Kolgan, [21], introduced for the first time a non linear high order scheme that circumvents Godunov's theorem. In order to do that, he proposed the use of limited slopes in the reconstruction of the conservative values used to build the flux function. Following this work the CVC Kolgan-type scheme was introduced in [54] and [23] for the shallow water equations. The new scheme, which is second order accuracy in space and first order in time, can be extended to the resolution of the Navier-stokes equations. This method is based on the idea of replacing the conservative values $\mathbf{W}_i^n$, $\mathbf{W}_j^n$ in the numerical viscosity by improved interpolations given by $\mathbf{W}_{iL}^n$, $\mathbf{W}_{jR}^n$ at both sides of each face Γ_{ij},

$$\mathbf{W}_{iL}^n = \mathbf{W}_i^n + \Delta^{ijL}, \quad \mathbf{W}_{jR}^n = \mathbf{W}_j^n - \Delta^{ijR},$$

where Δ^{ijL} and Δ^{ijR} are the left and right limited slopes at the face defined through the Galerkin gradients computed on the upwind tetrahedra, T_{ijL} and T_{ijR}, respectively (see Figure 2 for the 2D case). Moreover, we avoid spurious oscillations by taking into account a minmod-type limiter (see [21]):

$$\Delta^{ijL} = Lim\left(\frac{1}{2}\left(\nabla\mathbf{W}^n\right)_{T_{ijL}}\overline{N_iN_j}, \mathbf{W}_j^n - \mathbf{W}_i^n\right), \tag{36}$$

$$\Delta^{ijR} = Lim\left(\frac{1}{2}\left(\nabla\mathbf{W}^n\right)_{T_{ijR}}\overline{N_iN_j}, \mathbf{W}_j^n - \mathbf{W}_i^n\right). \tag{37}$$

Following [23], this high-order extrapolation is used only in the upwind contribution of the numerical flux retaining the conservative variables in the centred part. So that, the numerical flux reads

$$\phi\left(\mathbf{W}_i^n, \mathbf{W}_j^n, \mathbf{W}_{iL}^n, \mathbf{W}_{jR}^n, \boldsymbol{\eta}_{ij}\right)$$

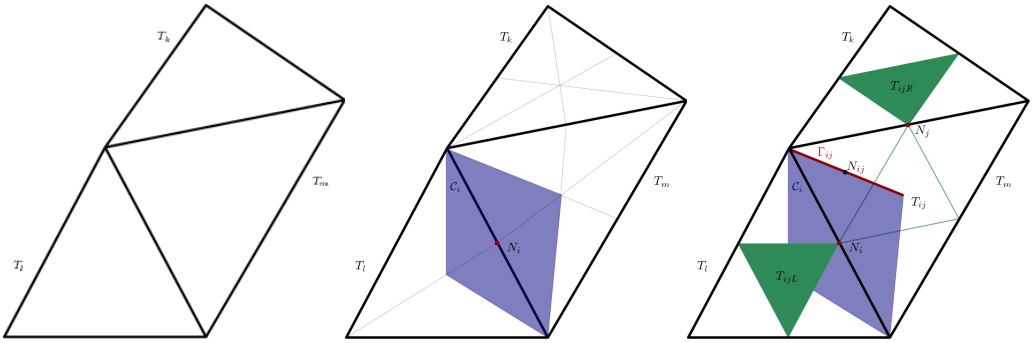

Figure 2: Construction of a dual 2D mesh and auxiliary triangles. Left: Finite elements of the original triangular mesh (black). Centre: Finite volume C_i (purple). Right: Upwind triangles (green).

$$= \frac{1}{2}\left(\mathcal{Z}(\mathbf{W}_i^n, \boldsymbol{\eta}_{ij}) + \mathcal{Z}(\mathbf{W}_j^n, \boldsymbol{\eta}_{ij})\right) - \frac{1}{2}\alpha_{RS}\left((\mathbf{W}_{iL}^n, \mathbf{W}_{jR}^n, \boldsymbol{\eta}_{ij}\right)\left(\mathbf{W}_{jR}^n - \mathbf{W}_{iL}^n\right). \tag{38}$$

3.3.2. LADER

ADER methodology, first put forward in [32] for the linear advection equation on Cartesian meshes and extended, for the one-dimensional case, in [50] to account for the diffusion and reaction terms, is applied in order to obtain a second order in time and space scheme. More precisely, a modification of the method is proposed to profit from the dual mesh structure to reduce the size of the stencil and, hence, the computational cost. Due to the small neighbourhood involved on the calculations related to each node, we will name this new scheme as LADER. The LADER scheme for the one-dimensional advection-diffusion-reaction equation is presented in Appendix A; the stability and truncation error analysis are also given.

To extend LADER to the three dimensional case four relevant issues must be taken into account:

1. The advection depends on the diffusion terms. That is, within the computation of the flux we will use Cauchy-Kovalevskaya procedure to obtain evolved values for the variables which contain information from both terms.
2. The evolved variables obtained for computing the diffusion term neglect the presence of the advection term.

3. As a consecuence of 1 and 2, advection and diffusion terms need to be computed using the proper evolved variables, which will be different for each of them.
4. To compute the gradients needed to obtain the evolved variables we can profit from the FE mesh and use a Galerkin approach.

In this section, for ease of comprehension, we will assume that the diffusion term only accounts for the velocity gradient, the remaining terms can be computed analogously. Let us consider W an approximation of a scalar conservative variable and α the related diffusion coefficient, the proposed method includes the following steps:

Step 1. Data reconstruction. Reconstruction of the data in terms of first degree polynomials is considered. At each finite volume we define four polynomials each of them at the neighbourhood of one of the boundary faces. Focusing on a face Γ_{ij} its two related reconstruction polynomials are

$$p_{ij}^{i}(N) = W_i + (N - N_i)\,(\nabla W)_{ij}^{i}\,, \quad p_{ij}^{j}(N) = W_j + (N - N_j)\,(\nabla W)_{ij}^{j}\,. \tag{39}$$

A possible election of the gradients is

$$(\nabla W)_{ij}^{i} = \nabla W_{T_{ijL}}, \quad (\nabla W)_{ij}^{j} = \nabla W_{T_{ijR}}. \tag{40}$$

which will result on a linear reconstruction as it is based on a fixed stencil.

In order to circumvent Godunov's theorem and prevent spurious oscillations, a non-linear reconstruction is considered (see [2]). More precisely, the ENO (Essentially Non-Oscillatory) interpolation method is applied. The slopes are adaptively chosen as follows:

$$(\nabla W)_{ij}^{i} = \begin{cases} (\nabla W)_{T_{ijL}} & \text{if } \left|(\nabla W)_{T_{ijL}} \cdot (N_{ij} - N_i)\right| \leq \left|(\nabla W)_{T_{ij}} \cdot (N_{ij} - N_i)\right|, \\ (\nabla W)_{T_{ij}} & \text{if } \left|(\nabla W)_{T_{ijL}} \cdot (N_{ij} - N_i)\right| > \left|(\nabla W)_{T_{ij}} \cdot (N_{ij} - N_i)\right|; \end{cases}$$

$$(\nabla W)_{ij}^{j} = \begin{cases} (\nabla W)_{T_{ijR}} & \text{if } \left|(\nabla W)_{T_{ijR}} \cdot (N_{ij} - N_j)\right| \leq \left|(\nabla W)_{T_{ij}} \cdot (N_{ij} - N_j)\right|, \\ (\nabla W)_{T_{ij}} & \text{if } \left|(\nabla W)_{T_{ijR}} \cdot (N_{ij} - N_j)\right| > \left|(\nabla W)_{T_{ij}} \cdot (N_{ij} - N_j)\right|; \end{cases}$$

where $(\nabla W)_{T_{ij}}$ is the gradient of the velocity at the auxiliary tetrahedra which intersects the face.

Step 2. Computation of boundary extrapolated values at the barycenter of the faces, N_{ij}:

$$W_{i\,N_{ij}} = p^i_{ij}(N_{ij}) = W_i + (N_{ij} - N_i)\,(\nabla W)^i_{ij}\,, \tag{41}$$

$$W_{j\,N_{ij}} = p^j_{ij}(N_{ij}) W_j + (N_{ij} - N_j)\,(\nabla W)^j_{ij}\,. \tag{42}$$

Step 3. Computation of the flux terms with second order of accuracy using the mid-point rule. Taylor series expansion in time and Cauchy-Kovalevskaya procedure are applied to locally approximate the conservative variables at time $\frac{\Delta t}{2}$. This methodology accounts for the contribution of the advection and diffusion terms to the time evolution of the flux term. The resulting evolved variables read

$$\begin{aligned}\overline{W_{i\,N_{ij}}} &= W_{i\,N_{ij}} - \frac{\Delta t}{2\mathcal{L}_{ij}}\left(\mathcal{Z}(W_{i\,N_{ij}}, \boldsymbol{\eta}_{ij}) + \mathcal{Z}(W_{j\,N_{ij}}, \boldsymbol{\eta}_{ij})\right)\\ &+\frac{\Delta t}{2\mathcal{L}^2_{ij}}\left(\alpha_{iN_{ij}}\,(\nabla W)^i_{ij}\,\boldsymbol{\eta}_{ij} + \alpha_{jN_{ij}}\,(\nabla W)^j_{ij}\,\boldsymbol{\eta}_{ij}\right),\end{aligned} \tag{43}$$

$$\begin{aligned}\overline{W_{j\,N_{ij}}} &= W_{j\,N_{ij}} - \frac{\Delta t}{2\mathcal{L}_{ij}}\left(\mathcal{Z}(W_{i\,N_{ij}}, \boldsymbol{\eta}_{ij}) + \mathcal{Z}(W_{j\,N_{ij}}, \boldsymbol{\eta}_{ij})\right)\\ &+\frac{\Delta t}{2\mathcal{L}^2_{ij}}\left(\alpha_{iN_{ij}}\,(\nabla W)^i_{ij}\,\boldsymbol{\eta}_{ij} + \alpha_{jN_{ij}}\,(\nabla W)^j_{ij}\,\boldsymbol{\eta}_{ij}\right).\end{aligned} \tag{44}$$

We have denoted $\mathcal{L}_{ij} = \min\left\{\frac{|C_i|}{\mathrm{S}(C_i)}, \frac{|C_j|}{\mathrm{S}(C_j)}\right\}$ with $\mathrm{S}(C_i)$ the area of the surface of cell C_i. Two different options will be considered in the scheme concerning the evolved variables. The first one corresponds to the previous definition of the evolved variables. Meanwhile, the second one neglects the evolution of the diffusion term.

Step 4. Computation of the numerical flux considering Rusanov scheme.

$$\begin{aligned}\phi\left(\overline{W^n_{i\,N_{ij}}}, \overline{W^n_{j\,N_{ij}}}, \boldsymbol{\eta}_{ij}\right) &= \frac{1}{2}\left(\mathcal{Z}\left(\overline{W^n_{i\,N_{ij}}}, \boldsymbol{\eta}_{ij}\right) + \mathcal{Z}\left(\overline{W^n_{j\,N_{ij}}}, \boldsymbol{\eta}_{ij}\right)\right)\\ &-\frac{1}{2}\alpha_{RS}\left(\overline{W^n_{i\,N_{ij}}}, \overline{W^n_{j\,N_{ij}}}, \boldsymbol{\eta}_{ij}\right)\left(\overline{W^n_{j\,N_{ij}}} - \overline{W^n_{i\,N_{ij}}}\right).\end{aligned} \tag{45}$$

3.4. Viscous terms

We come next to describe the computation of the integrals involving the viscous terms. First, applying Gauss' theorem we relate the volume integral

of the diffusion term with a surface integral over the boundary, Γ_i. Next, this integral is split into the integrals over the cell interfaces Γ_{ij}. Thus, the viscous term of the momentum conservation equation reads

$$\int_{C_i} \mathrm{div}\tau^n \mathrm{dV} = \sum_{N_j \in \mathcal{K}_i} \int_{\Gamma_{ij}} \tau^n \tilde{\boldsymbol{\eta}}_{ij}\, \mathrm{dS}$$

$$= \sum_{N_j \in \mathcal{K}_i} \int_{\Gamma_{ij}} \left[(\mu + \mu_t^n) \left(\nabla \mathbf{U}^n + (\nabla \mathbf{U}^n)^T \right) - \frac{2}{3} \rho K^n I \right] \widetilde{\boldsymbol{\eta}}_{ij}\, \mathrm{dS}. \tag{46}$$

Two different approaches can be considered in order to compute the above integral.

On the one hand, decomposition with semi-implicit and explicit discretizations can be applied when using the CVC Kolgan-type scheme. This methodology splits the diffusion flux into its orthogonal and non-orthogonal parts and relax the stability condition on the time step size (see [1] for further details).

On the other hand, the dual mesh ease the use of Galerkin approach to compute the derivatives involved in (46). We introduce a numerical diffusion function $\varphi_{\mathbf{u}}$ such that

$$\int_{\Gamma_{ij}} (\mu + \mu_t^n) \nabla \mathbf{U}^n \tilde{\boldsymbol{\eta}}_{ij} \mathrm{dS} \approx \varphi_{\mathbf{u}} \left(\mathbf{U}_i^n, \mathbf{U}_j^n, \mu_{t,\,i}^n, \mu_{t,\,j}^n, \boldsymbol{\eta}_{ij} \right) \tag{47}$$

and we consider

$$\varphi_{\mathbf{u}} \left(\mathbf{U}_i^n, \mathbf{U}_j^n, \mu_{t,\,i}^n, \mu_{t,\,j}^n, \boldsymbol{\eta}_{ij} \right) = \left(\mu + \mu_{t,\,ij}^n \right) \left(\nabla \mathbf{U}^n \right)_{T_{ij}} \boldsymbol{\eta}_{ij}, \tag{48}$$

with

$$\mu_{t,\,ij}^n = \frac{1}{2} \left(\mu_{t,\,i}^n + \mu_{t,\,j}^n \right). \tag{49}$$

Since we know the value of the turbulent kinetic energy at the nodes of the finite volumes, we approximate the turbulent kinetic energy term as the average of the values obtained at the two nodes related to the face

$$-\int_{\Gamma_{ij}} \frac{2}{3} W_k^n \tilde{\boldsymbol{\eta}}_{ij} \mathrm{dS} = -\frac{1}{3} \left(W_{k,\,i}^n + W_{k,\,j}^n \right) \boldsymbol{\eta}_{ij}. \tag{50}$$

Finally, the viscous terms for the remaining equations are obtained equally to the gradient term of the momentum equation:

$$\int_{C_i} \frac{1}{\rho} \mathrm{div}\left(\boldsymbol{\mathcal{D}}^n \nabla \widehat{\mathbf{W}}^n\right) \mathrm{dV} = \frac{1}{\rho} \sum_{N_j \in \mathcal{K}_i} \int_{\Gamma_{ij}} \boldsymbol{\mathcal{D}}^n \nabla \widehat{\mathbf{W}}^n \, \tilde{\boldsymbol{\eta}}_{ij} \, \mathrm{dS}, \tag{51}$$

where

$$\boldsymbol{\mathcal{D}}^n = \begin{pmatrix} \mathcal{D}_k^n & 0 & 0 \\ 0 & \mathcal{D}_\varepsilon^n & 0 \\ 0 & 0 & \mathcal{D}_{\mathbf{y}}^n \end{pmatrix} = \begin{pmatrix} \mu + \dfrac{\mu_t^n}{\sigma_k} & 0 & 0 \\ 0 & \mu + \dfrac{\mu_t^n}{\sigma_\varepsilon} & 0 \\ 0 & 0 & \rho\mathcal{D} + \dfrac{\mu_t^n}{Sc_t} \end{pmatrix}. \tag{52}$$

Thus, we can introduce the diffusion flux function, $\varphi_{\widehat{\mathbf{w}}}$, verifying

$$\begin{aligned} &\int_{\Gamma_{ij}} \boldsymbol{\mathcal{D}}^n \nabla \widehat{\mathbf{W}}^n \tilde{\boldsymbol{\eta}}_{ij} \mathrm{dS} \approx \varphi_{\widehat{\mathbf{w}}}\left(\widehat{\mathbf{W}}_i^n, \widehat{\mathbf{W}}_j^n, \mu_{t,\,i}^n, \mu_{t,\,j}^n, \boldsymbol{\eta}_{ij}\right), \\ &\varphi_{\widehat{\mathbf{w}}}\left(\widehat{\mathbf{W}}_i^n, \widehat{\mathbf{W}}_j^n, \mu_{t,\,i}^n, \mu_{t,\,j}^n, \boldsymbol{\eta}_{ij}\right) = \boldsymbol{\mathcal{D}}_{ij}^n \left(\nabla \widehat{\mathbf{W}^n}\right)_{T_{ij}} \boldsymbol{\eta}_{ij} \end{aligned} \tag{53}$$

The above methodologies are used to approximate the viscous terms when choosing a first order method or the CVC Kolgan-type scheme to compute the advection term. Nevertheless, the LADER methodology requires a special treatment.

3.4.1. LADER approach: the viscous terms

As was already introduced in Section 3.3.2, to apply LADER and to obtain a second order in space and time scheme, instead of computing the diffusion flux functions, $\varphi_{\mathbf{u}}$ and $\varphi_{\widehat{\mathbf{W}}}$, with the value of the variables at the previous time step, $\mathbf{U}^n$, K^n, E^n and $\mathbf{Y}^n$, its is necessary to use some evolved values, $\overline{\mathbf{U}^n}$, $\overline{K^n}$, $\overline{E^n}$ and $\overline{\mathbf{Y}^n}$.

It is important to remark that the former evolved variables do not match the already computed ones for the flux term (see Appendix A for a detailed analysis of the scalar advection-diffusion-reaction equation). Taylor series expansion in time and Cauchy-Kovalevskaya procedure are applied neglecting the advection term so that a second order in space and time scheme is attained:

$$\overline{\mathbf{U}^n} = \mathbf{U}^n + \frac{\Delta t}{2}\left\{\mathrm{div}\left[\left(\mu + \mu_t^n\right)\nabla \mathbf{U}^n - \frac{2}{3}\rho K^n \mathbf{I}\right]\right\}, \tag{54}$$

$$\overline{K^n} = K^n + \frac{\Delta t}{2}\left[\left(\mu + \frac{\mu_t^n}{\sigma_k}\right)\nabla K^n\right], \tag{55}$$

$$\overline{E^n} = E^n + \frac{\Delta t}{2}\left[\left(\mu + \frac{\mu_t^n}{\sigma_\varepsilon}\right)\nabla E^n\right], \tag{56}$$

$$\overline{\mathbf{Y}^n} = \mathbf{Y}^n + \frac{\Delta t}{2}\left[\left(\rho\mathcal{D} + \frac{\mu_t^n}{Sc_t}\right)\nabla \mathbf{Y}^n\right]. \tag{57}$$

In what follows, we describe the computation of the evolved velocities at an arbitrary node N_i:

1. The gradients of the original variables are computed at each auxiliary tetrahedra of the FE mesh, T_{ij} (see, on the 2D representation in Figure 2, the triangle with green contour). The value of the gradient at each node, N_i, is obtained as the average of the values on the two tetrahedra containing the node, T_{ijL} (green filled triangle in Figure 2) and T_{ij}. Taking into account the viscosity coefficients and the turbulent kinetic energy term, we introduce the auxiliary variable:

$$\mathbf{V}_i^n := \left(\mu + \mu_{t,i}^n\right)\frac{1}{2}\left(\left(\nabla \mathbf{U}^n\right)_{T_{ijL}} + \left(\nabla \mathbf{U}^n\right)_{T_{ij}}\right) - \frac{2}{3}\rho K_i^n I. \tag{58}$$

2. The divergence is computed as the average of the divergences of $\mathbf{V}^n$ obtained on the auxiliary tetrahedra:

$$\overline{\mathbf{U}_i^n} = \mathbf{U}_i^n + \frac{\Delta t}{4}\mathrm{tr}\left(\left(\nabla \mathbf{V}^n\right)_{T_{ijL}} + \left(\nabla \mathbf{V}^n\right)_{T_{ij}}\right). \tag{59}$$

3. The diffusion function $\varphi_{\mathbf{u}}$ is evaluated on the evolved variables:

$$\varphi_{\mathbf{u}}\left(\overline{\mathbf{U}_i^n}, \overline{\mathbf{U}_j^n}, \mu_{t,i}^n, \mu_{t,j}^n, \boldsymbol{\eta}_{ij}\right) = \left(\mu + \mu_{t,ij}^n\right)\left(\nabla \overline{\mathbf{U}^n}\right)_{T_{ij}}\boldsymbol{\eta}_{ij}. \tag{60}$$

The remaining evolved variables are similarly obtained. Hence the related diffusion function reads

$$\varphi_{\widehat{\mathbf{w}}}\left(\overline{\widehat{\mathbf{W}}_i^n}, \overline{\widehat{\mathbf{W}}_j^n}, \mu_{t,i}^n, \mu_{t,j}^n, \boldsymbol{\eta}_{ij}\right) = \boldsymbol{\mathcal{D}}_{ij}^n\left(\nabla \overline{\widehat{\mathbf{W}}^n}\right)_{T_{ij}}\boldsymbol{\eta}_{ij}. \tag{61}$$

3.5. Pressure term

For the integral of the pressure gradient we follow [1]. We split the boundary Γ_i into the cell interfaces Γ_{ij} using Gauss' theorem and we compute the pressure as the arithmetic mean of its values at the three vertices of face Γ_{ij} and the barycentre of the tetrahedra to which the face belongs. Then, the corresponding approximation of the integral is given by

$$\int_{\Gamma_{ij}} \pi^n \widetilde{\boldsymbol{\eta}}_{ij}\mathrm{dS} \approx \left[\frac{5}{12}\left(\pi^n(V_1) + \pi^n(V_2)\right) + \frac{1}{12}\left(\pi^n(V_3) + \pi^n(V_4)\right)\right]\boldsymbol{\eta}_{ij}. \tag{62}$$

3.6. Projection stage

Within the projection stage, the pressure is computed using a standard finite element method. The incremental projection method presented in [11] is adapted to solve (18)-(19) obtaining the following weak problem:

Find $\delta^{n+1} \in V_0 := \left\{ z \in H^1(\Omega) : \int_\Omega z = 0 \right\}$ *verifying*

$$\int_\Omega \nabla \delta^{n+1} \cdot \nabla z \, \mathrm{dV} = \frac{1}{\Delta t} \int_\Omega \widetilde{\mathbf{W}}^{n+1} \cdot \nabla z \, \mathrm{dV} - \frac{1}{\Delta t} \int_{\partial\Omega} G^{n+1} z \, \mathrm{dS} \quad \forall z \in V_0, \tag{63}$$

where $\delta^{n+1} := \pi^{n+1} - \pi^n$ (see [1] for further details).

3.7. Post-projection stage

Once the pressure is computed, we can update $\mathbf{W}_{\mathbf{u}}^{n+1}$ with $\nabla \delta_i^{n+1}$, that is,

$$\mathbf{W}_{\mathbf{u},\,i}^{n+1} = \widetilde{\mathbf{W}}_{\mathbf{u},\,i}^{n+1} + \Delta t \nabla \delta_i^{n+1}. \tag{64}$$

The previous computation of the updated velocities allows for an implicit approach of the production term G_k on the turbulence equations. Meanwhile, for the dissipative terms a semi-implicit scheme is used:

$$\frac{W_{k,\,i}^{n+1} - \widetilde{W}_{k,\,i}^{n+1}}{\Delta t} + W_{\varepsilon,\,i}^{n} - G_{k,\,i}(\mathbf{U}^{n+1}) = f_{k,\,i}^{n}, \tag{65}$$

$$\frac{W_{\varepsilon,\,i}^{n+1} - \widetilde{W}_{\varepsilon,\,i}^{n+1}}{\Delta t} + C_{2\varepsilon} \frac{W_{\varepsilon,\,i}^{n}}{W_{k,\,i}^{n}} W_{\varepsilon,\,i}^{n+1} - C_{1\varepsilon} \frac{W_{\varepsilon,\,i}^{n}}{W_{k,\,i}^{n}} G_{k,\,i}(\mathbf{U}^{n+1}) = f_{\varepsilon,\,i}^{n} \tag{66}$$

where the derivatives involved in the production term, $G_{k,\,i}(\mathbf{U}^{n+1})$, are computed as the averaged of the auxiliary tetrahedra related to the node N_i. Finally, the source terms $\mathbf{f}_{\widehat{\mathbf{w}}}$ are pointwise evaluated.

3.8. Boundary conditions

The boundary conditions were defined following [1]:

- Dirichlet boundary conditions for inviscid fluids: the normal component of the conservative variable is set at the boundary nodes.
- Dirichlet boundary conditions for viscous fluids: the value of the conservative variable is imposed at the boundary nodes.

- Neumann boundary conditions: the definition of $\widetilde{\mathbf{W}}^{n+1}$ takes into account the inflow/outflow boundary condition with no need for any additional treatment.

Moreover, in the manufactured tests designed to analyse the order of accuracy of the numerical discretizations, it is a usual practice to impose the values of the exact solution at the boundary nodes. This practice avoids that the accuracy of the method can be affected by the treatment of the boundary conditions. From the mathematical point of view, it is like considering Dirichlet boundary conditions.

4. Numerical results

In this section, we present the results obtained for several test problems. In order to define the time step, two different options are implemented in the code. On the one hand, we can simply introduce a fixed time step. On the other hand, we can provide the CFL from which the code will compute the time step at each time iteration. The latest option is the one chosen to run the test cases presented in this paper. Therefore, to determine the time step at each time iteration, we compute a local value for the time step at each cell C_i,

$$\Delta t_{C_i} = \frac{\mathrm{CFL}\,\mathcal{L}_{\mathrm{i}}^2}{2\,|\mathbf{U}_i|\,\mathcal{L}_i + \max\left\{\mu + \mu_{t,\,i}, \rho\mathcal{D} + \dfrac{\mu_{t,\,i}}{Sc_t}\right\}} \tag{67}$$

with $\mathcal{L}_i := \frac{|C_i|}{\mathrm{S}(C_i)}$. Finally, as global time step at each time iteration, Δt, we choose the minimum time steps obtained at each cell.

Remark 1. *The above definition of Δt_{C_i} is valid if the transport of species equation is solved, otherwise its value is given by*

$$\Delta t_{C_i} = \frac{\mathrm{CFL}\,\mathcal{L}_{\mathrm{i}}^2}{2\,|\mathbf{U}_i|\,\mathcal{L}_i + \mu + \mu_{t,\,i}}. \tag{68}$$

4.1. Manufactured test 1. Laminar flow

The first test to be posed was obtained using the method of the manufactured solutions (MMS). We consider the domain $\Omega = [0, 1]^3$ and we assume the flow being defined by

$$\rho = 1, \tag{69}$$

$$\pi(x, y, z, t) = \cos(\pi t(x + y + z)), \tag{70}$$

$$\mathbf{u}(x, y, z, t) = \left(\sin(\pi y t)\cos(\pi z t),\ -\cos(\pi z^3 t),\ \exp(-2\pi x t^2)\right)^T, \tag{71}$$

with $\mu = 10^{-2}$. The related source terms are included in Appendix B.

To perform the error and order of accuracy analysis we employ the three uniform meshes with different cell sizes presented in Table 1. We have de-

Mesh	N	Elements	Vertices	Nodes	V_h^m (m^3)	V_h^M (m^3)
M_1	4	384	125	864	$6.51E-04$	$1.30E-03$
M_2	8	3072	729	6528	$8.14E-05$	$1.63E-04$
M_3	16	24576	4913	50688	$1.02E-05$	$2.03E-05$

Table 1: Manufactured test 1. Laminar flow. Mesh features.

noted $N+1$ the number of points along the edges, $h = 1/N$, V_h^m the minimum volume of the finite volumes and V_h^M the maximum volume of the finite volumes.

Four different methods are used to solve the problem: the first order method presented in [1], CVC method with an orthogonal decomposition of the diffusion term (CVC-orth), CVC method combined with a Galerkin approach for the diffusion term (CVC-G) and LADER. The errors and orders, depicted in Table 2, were computed as follows:

$$E(\pi)_{M_i} = \|\pi - \pi_{M_i}\|_{l^2(L^2(\Omega))} \quad E(\mathbf{w_u})_{M_i} = \|\mathbf{w_u} - \mathbf{w_u}_{M_i}\|_{l^2(L^2(\Omega)^3)}, \tag{72}$$

$$o_{\pi_{M_i/M_j}} = \frac{\log\left(E(\pi)_{M_i}/E(\pi)_{M_j}\right)}{\log\left(h_{M_i}/h_{M_j}\right)}, \quad o_{\mathbf{w_u}\,M_i/M_j} = \frac{\log\left(E(\mathbf{w_u})_{M_i}/E(\mathbf{w_u})_{M_j}\right)}{\log\left(h_{M_i}/h_{M_j}\right)}. \tag{73}$$

We can observe that CVC-G method provides an order of convergence close to two. This is in accordance with the theoretical order of this scheme, first order in time and second order in space, and the high time-dependency of the solution. Whereas, with LADER the expected second order of accuracy is achieved.

Method	Variable	E_{M_1}	E_{M_2}	E_{M_3}	o_{M_1/M_2}	o_{M_2/M_3}
Order 1	π	$1.24E-01$	$5.70E-02$	$2.96E-02$	1.12	0.95
	$\mathbf{w_u}$	$6.40E-02$	$3.32E-02$	$1.78E-02$	0.95	0.90
CVC-orth.	π	$6.30E-02$	$1.91E-02$	$8.84E-03$	1.72	1.11
	$\mathbf{w_u}$	$5.51E-02$	$2.06E-02$	$8.95E-03$	1.42	1.20
CVC-G	π	$5.98E-02$	$1.58E-02$	$4.58E-03$	1.92	1.78
	$\mathbf{w_u}$	$5.41E-02$	$1.88E-02$	$6.52E-03$	1.52	1.53
LADER	π	$4.10E-02$	$8.74E-03$	$2.03E-03$	2.23	2.11
	$\mathbf{w_u}$	$2.61E-02$	$5.76E-03$	$1.24E-03$	2.18	2.22

Table 2: Manufactured test1. Laminar flow. Observed errors and convergence rates. CFL = 1.

4.2. Manufactured test 2. Turbulent flow with species transport

The second academic test to be considered is a modification of Test 1 to account for the turbulence and species transport equations. Let us define the flow as

$$\rho = 1, \tag{74}$$

$$\pi(x, y, z, t) = \cos(\pi t(x + y + z)), \tag{75}$$

$$\mathbf{u}(x, y, z, t) = \left(\sin(\pi y t)\cos(\pi z t),\ -\cos(\pi z^3 t),\ \exp(-2\pi x t^2)\right)^T, \tag{76}$$

$$k(x, y, z, t) = \sin(\pi x t) + 2, \tag{77}$$

$$\varepsilon(x, y, z, t) = \exp(-\pi z t) + 1, \tag{78}$$

$$y(x, y, z, t) = \sin(\pi x t) + 2. \tag{79}$$

with parameters $\mu = 10^{-2}$, $\mathcal{D} = 10^{-3}$. For the exact solution to verify the equations, taught expressions of the source terms have to be taken. They have been included in Appendix B.

We consider the meshes already defined in Table 1 and a CFL = 10 (the reason why this large value of CFL is admitted was studied in [50]). Dirichlet boundary conditions are set for all the equations on the boundary. The computed errors are presented in Table 3. The results obtained for CVC-orth confirm that using only second order in space for computing the flux terms and neglecting the non orthogonal component will not capture properly the turbulence. Second order in space must also be used to approximate the diffusion terms and the whole flux should be computed. Furthermore, a second order in time scheme improves the results and order attained.

Method	Variable	E_{M_1}	E_{M_2}	E_{M_3}	o_{M_1/M_2}	o_{M_2/M_3}
Order 1	π	$6.97E-01$	$5.52E-01$	$4.93E-01$	0.34	0.16
	$\mathbf{w_u}$	$4.40E-02$	$2.80E-02$	$2.18E-02$	0.65	0.36
	w_k	$3.85E-02$	$2.45E-02$	$2.09E-02$	0.65	0.23
	w_ε	$1.53E-02$	$8.47E-03$	$6.40E-03$	0.85	0.40
	w_y	$2.93E-02$	$2.04E-02$	$1.76E-02$	0.52	0.21
CVC-orth.	π	$6.23E-01$	$5.13E-01$	$4.75E-01$	0.28	0.11
	$\mathbf{w_u}$	$4.08E-02$	$2.65E-02$	$2.10E-02$	0.62	0.33
	w_k	$3.18E-02$	$2.13E-02$	$1.95E-02$	0.58	0.13
	w_ε	$1.51E-02$	$8.17E-03$	$6.15E-03$	0.89	0.41
	w_y	$2.51E-02$	$1.85E-02$	$1.68E-02$	0.44	0.14
CVC-G	π	$2.70E-01$	$7.60E-02$	$2.09E-02$	1.83	1.86
	$\mathbf{w_u}$	$1.50E-02$	$5.18E-03$	$1.49E-03$	1.54	1.80
	w_k	$1.54E-02$	$3.24E-03$	$8.22E-04$	2.25	1.98
	w_ε	$1.06E-02$	$2.39E-03$	$6.35E-04$	2.15	1.91
	w_y	$7.27E-03$	$1.89E-03$	$4.86E-04$	1.94	1.96
LADER	π	$2.68E-01$	$7.61E-02$	$2.10E-02$	1.82	1.86
	$\mathbf{w_u}$	$1.51E-02$	$5.17E-03$	$1.50E-03$	1.55	1.79
	w_k	$1.37E-02$	$2.51E-03$	$5.89E-04$	2.45	2.09
	w_ε	$9.87E-03$	$1.80E-03$	$4.09E-04$	2.46	2.14
	w_y	$7.25E-03$	$1.60E-03$	$3.79E-04$	2.18	2.08

Table 3: Manufactured test 2. Turbulent flow. Observed errors and convergence rates. CFL = 10.

4.3. Test 3. Gaussian sphere

The next problem to be analysed is the Gaussian sphere test introduced in [55] and [17]. We consider a normal distribution function in the domain $\Omega = [-0.9, 0.9] \times [-0.9, 0.9] \times [-0.3, 0.3]$ with standard deviation 0.08 and mean 0.25. The density is one, the velocity vector is defined as $\mathbf{u}(x, y, z, t) = (-y,\ x,\ 0)^T$ and we assume that the diffusion matrix is given by $\mathcal{D} = \mu$. Hence, the solution of the problem is given by

$$\mathrm{y}(x, y, z, t) = \left(\frac{\sigma_0}{\sigma(t)}\right)^3 \exp\left(\frac{-r}{2\sigma(t)^2}\right) \tag{80}$$

with

$$r(x, y, z, t) = (\bar{x} + 0.25)^2 + \bar{y}^2 + z^2, \quad \sigma(t) = \sqrt{\sigma_0^2 + 2t\mathcal{D}}, \tag{81}$$

$$\bar{x} = x\cos(t) + y\sin(t), \quad \bar{y} = -x\sin(t) + y\cos(t). \tag{82}$$

The flow definition is completed setting the source terms

$$\mathbf{f}_{\mathbf{u}}(x, y, z, t) = (-x, -y, 0)^T, \quad f_{\mathrm{y}}(x, y, z, t) = 0, \tag{83}$$

and considering Dirichlet boundary conditions.

In order to analyse the accuracy in time and space, five structured meshes were generated. The properties of these meshes can be seen in Table 4, where h denotes the size of the cubes used to generate the tetrahedra of the finite element mesh.

Mesh	Finite elements	Vertices	Nodes	h
M_1	11664	2527	24408	0.1
M_2	18522	3872	38514	0.0857
M_3	54000	10571	111000	0.06
M_4	93312	17797	190944	0.05
M_5	182250	33856	256711	0.04

Table 4: Test 3. Gaussian sphere. Mesh features.

Table 5 shows the results obtained for the test considering $\mu = 10^{-3}$. On the other hand, in Table 6 the errors and orders of accuracy for $\mu = 10^{-2}$ are presented. In both test cases we have assumed a final time $t_{\mathrm{end}} = 2\pi$

so that the sphere completes one revolution. Two different methodologies were considered to run these tests: CVC-G and LADER. We can observe that for $\mu = 10^{-3}$ CVC-G scheme only achieves first order and for $\mu = 10^{-2}$ the order obtained is a bit greater but still lower than two for the velocities approach. Meanwhile, using LADER we obtain the expected second order in both tests cases and the errors obtained decrease. These improvements are due to considering a second order method in time. The high diffusivity of the test makes necessary to consider second order in both, time and space, to achieve good approaches for all the unknowns of the problem.

The previous discussion is also consistent with the graphical results presented in Figures 3-8.

		π		$\mathbf{w_u}$		w_y	
		E_{M_i}	o_{M_{i-1}/M_i}	E_{M_i}	o_{M_{i-1}/M_i}	E_{M_i}	o_{M_{i-1}/M_i}
CVC-G	M_1	$7.48E-02$		$1.33E-01$		$4.00E-02$	
	M_2	$6.59E-02$	0.82	$1.17E-01$	0.84	$3.56E-02$	0.75
	M_3	$4.75E-02$	0.92	$8.52E-02$	0.89	$2.63E-02$	0.85
	M_4	$4.02E-02$	0.92	$7.21E-02$	0.91	$2.20E-02$	0.99
	M_5	$3.24E-02$	0.96	$5.82E-02$	0.96	$1.73E-02$	1.08
LADER	M_1	$1.02E-03$		$2.48E-03$		$2.31E-02$	
	M_2	$7.25E-04$	2.19	$1.81E-03$	2.02	$1.83E-02$	1.50
	M_3	$3.23E-04$	2.27	$8.17E-04$	2.24	$1.00E-02$	1.70
	M_4	$2.12E-04$	2.32	$5.41E-04$	2.26	$7.11E-03$	1.88
	M_5	$1.25E-04$	2.36	$3.24E-04$	2.30	$4.59E-03$	1.97

Table 5: Test 3. Gaussian sphere, $\mu = 10^{-3}$. Observed errors and convergence rates. CFL = 5 for CVC-G and CFL = 0.5 for LADER.

		π		$\mathbf{w_u}$		w_y	
		E_{M_i}	o_{M_{i-1}/M_i}	E_{M_i}	o_{M_{i-1}/M_i}	E_{M_i}	o_{M_{i-1}/M_i}
CVC-G	M_1	$3.31E-02$		$5.13E-02$		$2.19E-03$	
	M_2	$2.74E-02$	1.22	$4.29E-02$	1.16	$1.67E-03$	1.77
	M_3	$1.72E-02$	1.31	$2.74E-02$	1.26	$9.02E-04$	1.73
	M_4	$1.34E-02$	1.39	$2.15E-02$	1.34	$6.62E-04$	1.70
	M_5	$9.69E-03$	1.44	$1.57E-02$	1.40	$4.54E-04$	1.69
LADER	M_1	$3.68E-04$		$9.02E-04$		$1.61E-03$	
	M_2	$2.54E-04$	2.41	$6.24E-04$	2.02	$1.16E-03$	2.12
	M_3	$1.12E-04$	2.29	$2.60E-04$	2.24	$5.55E-04$	2.07
	M_4	$7.57E-05$	2.15	$1.66E-04$	2.26	$3.85E-04$	2.01
	M_5	$4.78E-05$	2.06	$9.54E-05$	2.30	$2.48E-04$	1.97

Table 6: Test 3. Gaussian sphere, $\mu = 10^{-2}$. Observed errors and convergence rates. CFL = 5 for CVC-G and CFL = 0.5 for LADER.

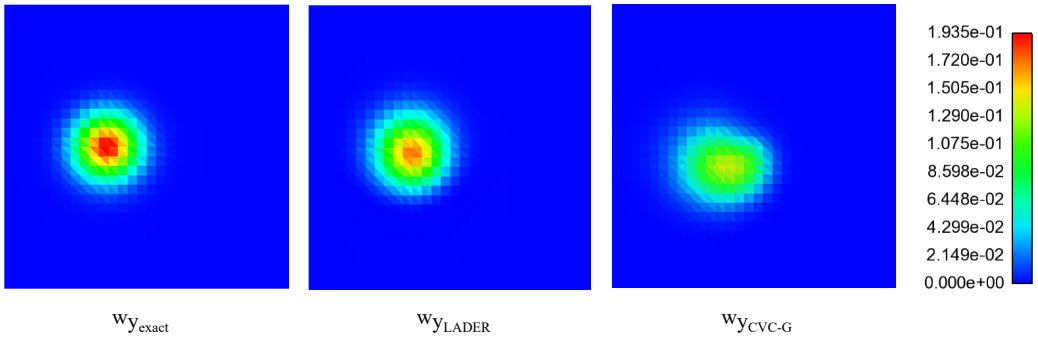

Figure 3: Test 3. Gaussian sphere, $\mu = 10^{-3}$. Contours of w_y at plane $z = 0$ using Mesh M_3. Left: exact solution. Centre: LADER. Right: CVC-G.

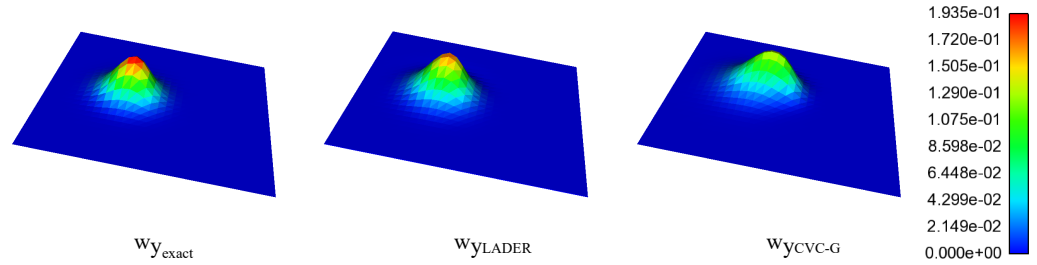

Figure 4: Test 3. Gaussian sphere, $\mu = 10^{-3}$. Elevated surfaces of w_y at plane $z = 0$ using Mesh M_3. Left: exact solution. Centred: LADER. Right: CVC-G.

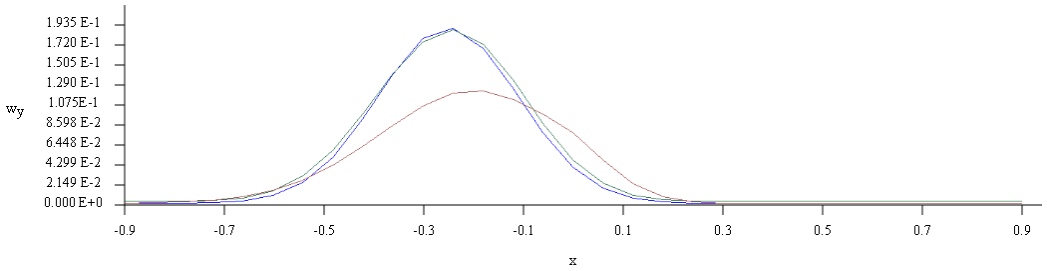

Figure 5: Test 3. Gaussian sphere, $\mu = 10^{-3}$. Profile of the exact solution (blue) and the computed solutions using LADER (green) and CVC-G (red) at plane $y = 0$.

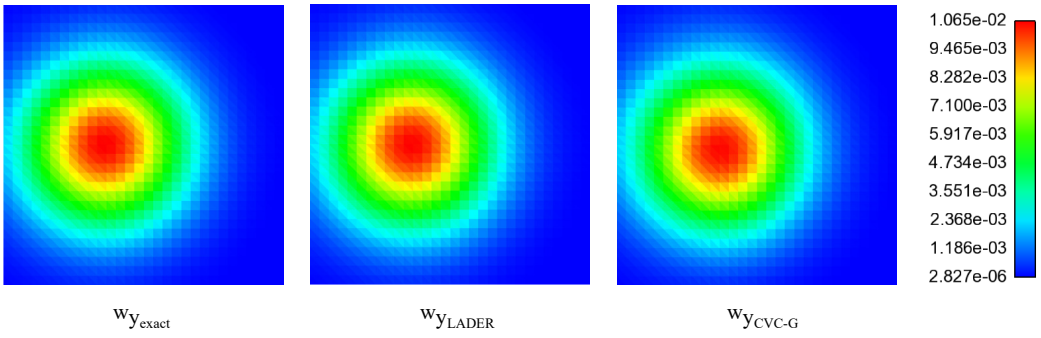

Figure 6: Test 3. Gaussian sphere, $\mu = 10^{-2}$. Contours of w_y at plane $z = 0$ using Mesh M_3. Left: exact solution. Centre: LADER. Right: CVC-G.

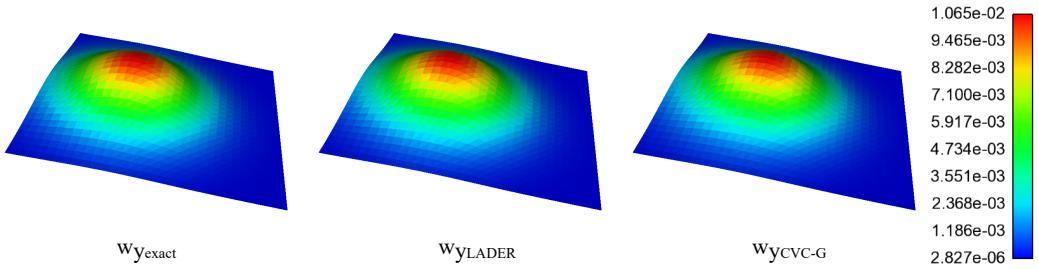

Figure 7: Test 3. Gaussian sphere, $\mu = 10^{-2}$. Elevated surfaces of w_y at plane $z = 0$ using Mesh M_3. Left: exact solution. Centre: LADER. Right: CVC-G.

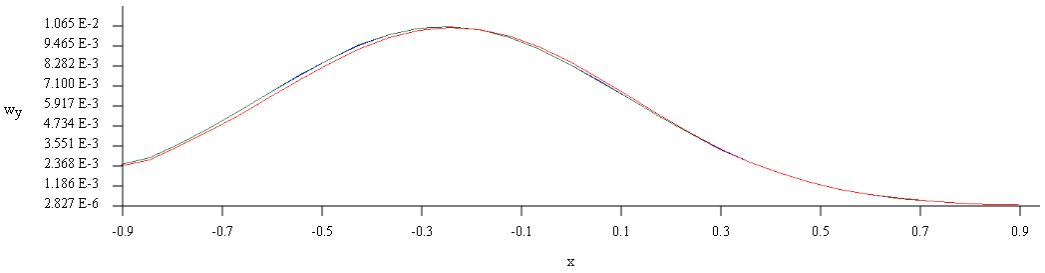

Figure 8: Test 3. Gaussian sphere, $\mu = 10^{-2}$. Profile of the exact solution (blue) and the computed solutions using LADER (green) and CVC-G (red) at plane $y = 0$.

4.4. Test 4. Flow around a cylinder

We consider the steady-state problem of a flow around a cylinder which has been introduced in [56] and employed, for instance, in [1] and [57] as a benchmark problem. The computational domain consists of a solid cylinder surrounded by a rectangular channel in which the flow evolves (see Figure 9). The dynamic viscosity of the fluid is $\mu = 10^{-3}$ and the inlet velocity has the form

$$\mathbf{u}(x, y, z, t) = \left(16Uyz(H - y)(H - z)/H^4, 0, 0\right)^T, \tag{84}$$

with $U = 0.45$, $H = 0.41$. Based on the viscosity, the cylinder diameter, $D = 0.1$, and an estimate of 0.2 for the mean inflow velocity, the flow has a Reynolds number of 20. At the outlet Neumann boundary conditions are considered. The mesh employed to obtain the numerical solution consists of 449746 finite elements and 909004 finite volumes.

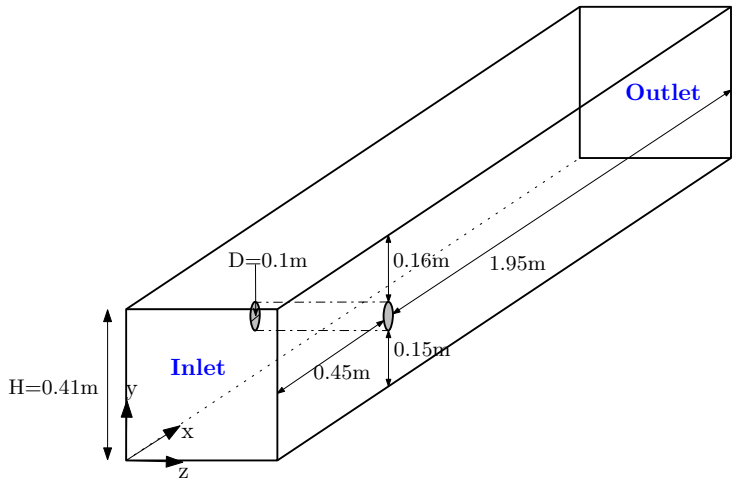

Figure 9: Test 4. Flow around a cylinder. Geometry.

The drag and lift coefficients for this problem are expressed by

$$c_d = \frac{500}{0.41} F_d, \;\; c_l = \frac{500}{0.41} F_l, \tag{85}$$

where F_d and F_l are the drag and lift forces, respectively:

$$F_d = \int_S \left(\mu \frac{\partial \mathbf{u}_\tau}{\partial \mathbf{n}_S} n_y - \pi n_x \right) \mathrm{dS}, \quad F_l = \int_S \left(-\mu \frac{\partial \mathbf{u}_\tau}{\partial \mathbf{n}_S} n_x - \pi n_y \right) \mathrm{dS} \tag{86}$$

with $\mathbf{n}_S = (n_x, n_y, 0)^t$ the inward pointing unit normal with respect to Ω, S the surface of the cylinder, and $\mathbf{n}_\tau = (n_y, -n_x, 0)^t$ one of the tangential vectors, the other one being $(0, 0, 1)^T$. The drag and lift forces were computed following [1]. As convergence criterion, at iteration k, we consider,

$$\frac{1}{\Delta t} \| \mathbf{W}_M^k - \mathbf{W}_M^{k-1} \|_{L^\infty(\Omega)^3} \leq 10^{-4}. \tag{87}$$

Method	Time iterations	C_D (min,max) $(6.05, 6.25)$	C_L (min,max) $(0.008, 0.01)$	$D\pi$ (min,max) $(0.165, 0.175)$
1. Order 1	1745	6.79	0.0062	0.1656
2. CVC-orth	72442	6.2463	-0.00067	0.1651
3. CVC-G	73994	6.1619	0.01996	0.1616
4. LADER	85638	6.1249	0.0161	0.1662

Table 7: Test 4. Flow around a cylinder. Obtained values for the aerodynamic coefficients and the pressure difference.

Four different simulations regarding the method employed were run:

Method 1: the first order method presented in [1], which considers the Rusanov scheme as the numerical flux.

Method 2: the second order in space and first order in time CVC-orth.

Method 3: CVC-G, also second order in space and first order in time.

Method 4: the second order method given by LADER.

The numerical results are summarized in Table 7. Along with the aerodynamic coefficients, the pressure difference $D\pi$ between the points $\mathbf{p}_1 = (0.45, 0.2, 0.205)$ and $\mathbf{p}_2 = (0.55, 0.2, 0.205)$, has been computed. We observe that the solutions obtained with the higher order method, as expected theoretically, are the most accurate with respect to the reference intervals obtained from the experimental data on [56]. Finally, Figures 10, 11 and 12 show the results obtained using LADER methodology.

Figure 10: Test 4. Flow around a cylinder. Pressure on $z = 0.205$.

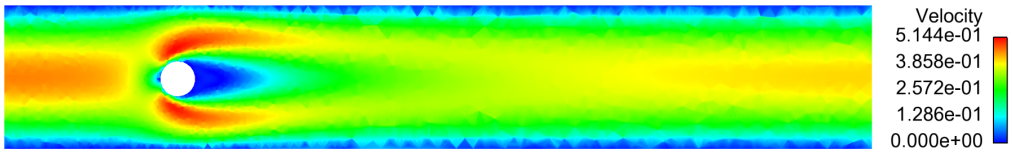

Figure 11: Test 4. Flow around a cylinder. Velocity magnitude on $z = 0.205$.

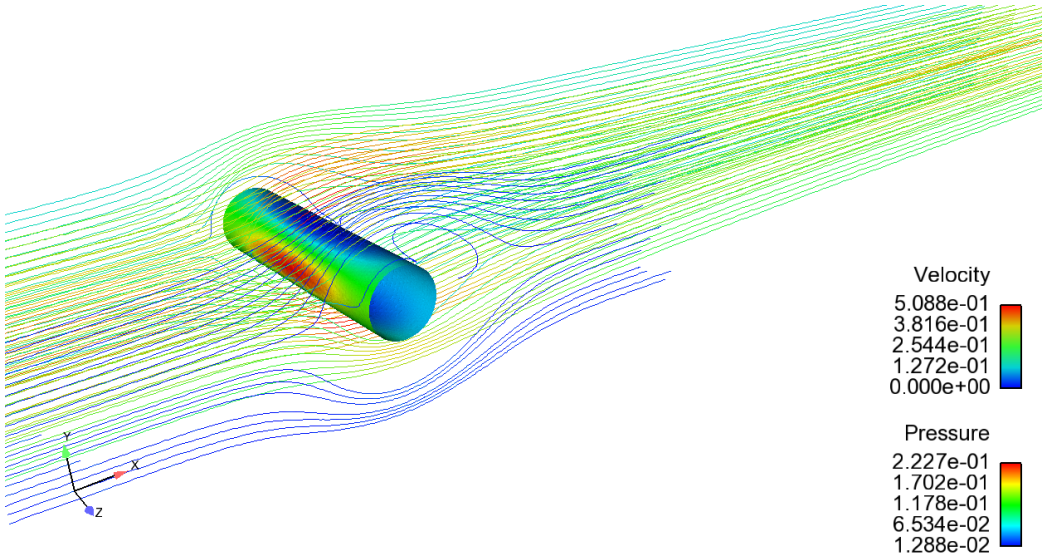

Figure 12: Test 4. Flow around a cylinder. Pressure over the cylinder and streamlines.

5. Summary and conclusions

In this paper a projection hybrid high order FV/FE method for incompressible flows has been presented. Navier-Stokes equations have been coupled with the $k - \varepsilon$ model in order to simulate turbulent flows. The system to be solved was enlarged with respect to [1] considering species transport. High order of accuracy has shown necessary for the proper computation of turbulent effects. Two different methodologies to achieve second order were presented. Firstly, CVC Kolgan provided a second order in space and first order in time scheme. To attain second order in space and time a new method was proposed: LADER. The corresponding accuracy and stability analysis were presented for the advection-diffusion-reaction equation. Godunov's theorem was circumvented thanks to an ENO-based approach. The computation of the gradients involved on diffusion terms was done via Galerkin.

The method was applied to manufactured test problems in order to asses the accuracy. Furthermore, different benchmarks were considered and the results obtained were successfully confronted with experimental data.

Acknowledgements

This work was financially supported by Spanish MICINN projects MTM2008-02483, CGL2011-28499-C03-01 and MTM2013-43745-R; by the Spanish MECD under grant FPU13/00279; by the Xunta de Galicia Consellería de Cultura Educación e Ordenación Universitaria under grant Axudas de apoio á etapa predoutoral do Plan I2C; by Xunta de Galicia and FEDER under research project GRC2013-014 and by Fundación Barrié under grant *Becas de posgrado en el extranjero*.

References

References

[1] A. Bermúdez, J. L. Ferrín, L. Saavedra, M. E. Vázquez-Cendón, A projection hybrid finite volume/element method for low-Mach number flows, J. Comp. Phys. 271 (2014) 360–378. doi:10.1016/j.jcp.2013.09.029. URL http://www.sciencedirect.com/science/article/pii/S0021999113006438

[2] E. F. Toro, Riemann solvers and numerical methods for fluid dynamics: A practical introduction, Springer, 2009. doi:10.1007/b79761.

[3] J. B. Bell, A. S. Day, A. S. Almgren, M. J. Lijewski, C. A. Rendleman, A parallel adaptive projection method for low Mach number flows, Int. J. Numer. Methods Fluids 40 (2002) 209–216. doi:10.1002/fld.310. URL http://onlinelibrary.wiley.com/doi/10.1002/fld.310/full

[4] R. B. Pember, A. S. Almgren, J. B. Bell, P. Colella, M. Howell, M. Lai, A high order projection method for the simulation of unsteady turbulent non premixed combustion in an industrial burner, in: Proceedings of the 8th International Symposium on Transport Phenomena in Combustion, 1995, pp. 16–20.

[5] A. Bermúdez, A. Dervieux, J. A. Desideri, M. E. Vázquez-Cendón, Upwind schemes for the two-dimensional shallow water equations with variable depth using unstructured meshes, Comput. Methods Appl. Mech. Eng. 155 (1) (1998) 49–72. doi:10.1016/S0045-7825(97)85625-3.

583 [6] T. Gallouët, L. Gastaldo, R. Herbin, J.-C. Latché, An uncondition-
584 ally stable pressure correction scheme for the compressible barotropic
585 Navier-Stokes equations, ESAIM: Mathematical Modelling and Numer-
586 ical Analysis 42 (2) (2008) 303–331. doi:10.1051/m2an:2008005.
587 URL https://doi.org/10.1051/m2an:2008005

588 [7] W. Gao, H. Li, R. Liu, An unstructured finite volume projection
589 method for pulsatile flows through an asymmetric stenosis, J. Eng.
590 Math. 72 (1) (2012) 125–140. doi:10.1007/s10665-011-9469-1.
591 URL https://link.springer.com/article/10.1007/s10665-011-9469-1

592 [8] S. Perron, S. Boivin, J.-M. Hérard, A finite volume method
593 to solve the 3D Navier-Stokes equations on unstructured col-
594 located meshes, Computers & fluids 33 (10) (2004) 1305–1333.
595 doi:https://doi.org/10.1016/j.compfluid.2003.10.006.
596 URL http://www.sciencedirect.com/science/article/pii/S004579300400057X

597 [9] S. Tu, S. Aliabadi, Development of a hybrid finite volume/element
598 solver for incompressible flows, Int. J. Numer. Methods Fluids 55 (2)
599 (2007) 177–203. doi:10.1002/fld.1454.
600 URL http://onlinelibrary.wiley.com/doi/10.1002/fld.1454/full

601 [10] S. Tu, S. Aliabadi, R. Patel, M. Watts, An implementation of the
602 Spalart-Allmaras DES model in an implicit unstructured hybrid finite
603 volume/element solver for incompressible turbulent flow, Int. J. Numer.
604 Methods Fluids 59 (9) (2009) 1051–1062. doi:10.1002/fld.1864.
605 URL http://onlinelibrary.wiley.com/doi/10.1002/fld.1864/abstract

606 [11] J. L. Guermond, P. Minev, J. Shen, An overview of projection methods
607 for incompressible flows, Comput. Methods Appl. Mech. Eng. 195 (2006)
608 6011–6045. doi:10.1016/j.cma.2005.10.010.

609 [12] E. F. Toro, A. Hidalgo, M. Dumbser, FORCE schemes on unstructured
610 meshes I: Conservative hyperbolic systems, J. Comput. Phys. 228 (9)
611 (2009) 3368 – 3389. doi:https://doi.org/10.1016/j.jcp.2009.01.025.
612 URL http://www.sciencedirect.com/science/article/pii/S0021999109000412

613 [13] M. Dumbser, A. Hidalgo, M. Castro, C. Parés, E. F. Toro, FORCE
614 schemes on unstructured meshes II: Non-conservative hyperbolic
615 systems, Comput. Methods Appl. Mech. Eng. 199 (2010) 625–647.

616 doi:https://doi.org/10.1016/j.cma.2009.10.016.
617 URL http://www.sciencedirect.com/science/article/pii/S0045782509003612

618 [14] M. Tavelli, M. Dumbser, A pressure-based semi-implicit space-
619 time discontinuous Galerkin method on staggered unstructured
620 meshes for the solution of the compressible Navier-Stokes equations
621 at all Mach numbers, J. Comput. Phys. 341 (2017) 341 – 376.
622 doi:https://doi.org/10.1016/j.jcp.2017.03.030.
623 URL http://www.sciencedirect.com/science/article/pii/S0021999117302255

624 [15] M. E. Vázquez-Cendón, Solving Hyperbolic Equations with Finite Vol-
625 ume Methods, Springer, 2015. doi:10.1007/978-3-319-14784-0.

626 [16] L. Cea, J. R. French, M. E. Vázquez-Cendón, Numerical modelling of
627 tidal flows in complex estuaries including turbulence: An unstructured
628 finite volume solver and experimental validation, Int. J. Numer. Meth.
629 Engng. 67 (2006) 1909–1932. doi:10.1002/nme.1702.
630 URL http://onlinelibrary.wiley.com/doi/10.1002/nme.1702/full

631 [17] L. Saavedra, Modelización matemática y resolución numérica de prob-
632 lemas de combustión de carbón pulverizado, Ph.D. thesis, Departa-
633 mento de Matemática Aplicada Universidade de Santiago de Compostela
634 (2011).

635 [18] P. Lax, B. Wendroff, Systems of conservation laws, Commun. Pur. Appl.
636 Math. 13 (2) (1960) 217–237. doi:10.1002/cpa.3160130205.

637 [19] P. D. Lax, Hyperbolic systems of conservation laws II, Commun. Pur.
638 Appl. Math. 10 (4) (1957) 537–566. doi:10.1002/cpa.3160100406.

639 [20] S. K. Godunov, A finite difference method for the computation of dis-
640 continuous solutions of the equations of fluid dynamics, Mat. Sb. 47
641 (1959) 357–393.

642 [21] V. Kolgan, Application of the principle of minimizing the derivative
643 to the construction of finite-difference schemes for computing discon-
644 tinuous solutions of gas dynamics, J. Comput. Phys. 230 (7) (2011)
645 2384–2390. doi:10.1016/j.jcp.2010.12.033.
646 URL http://www.sciencedirect.com/science/article/pii/S0021999110007072

[22] C. Berthon, Why the MUSCL-Hancock scheme is L1-stable, Numer. Math. 104 (2006) 27–46. doi:10.1007/s00211-006-0007-4.

[23] L. Cea, M. E. Vázquez-Cendón, Analysis of a new Kolgan-type scheme motivated by the shallow water equations, Appl. Num. Math. 62 (4) (2012) 489–506. doi:10.1016/j.apnum.2011.06.002.

[24] B. van Leer, On the relation between the upwind-differencing schemes of Godunov, Engquist-Osher and Roe, SIAM J. Sci. Stat. Comp. 5 (1) (1984) 1–20. doi:10.1137/0905001.

[25] B. van Leer, Towards the ultimate conservative difference scheme, J. Comp. Phys. 135 (2) (1997) 229–248, doi:10.1006/jcph.1997.5704.

[26] P. K. Sweby, High resolution schemes using flux limiters for hyperbolic conservation laws, SIAM J. Num. Anal. 21 (5) (1984) 995–1011. doi:10.1137/0721062.

[27] A. Harten, B. Engquist, S. Osher, S. R. Chakravarthy, Uniformly high order accurate essentially non-oscillatory schemes, III, in: Upwind and High-Resolution Schemes, Springer, 1987, pp. 218–290. doi:10.1006/jcph.1996.5632.

[28] C. E. Castro, E. F. Toro, Solvers for the high-order Riemann problem for hyperbolic balance laws, J. Comp. Phys. 227 (4) (2008) 2481–2513. doi:10.1016/j.jcp.2007.11.013.

[29] C.-W. Shu, S. Osher, Efficient implementation of essentially non-oscillatory shock-capturing schemes, J. Comp. Phys. 77 (2) (1988) 439–471. doi:10.1016/0021-9991(88)90177-5.

[30] X.-D. Liu, S. Osher, T. Chan, Weighted essentially non-oscillatory schemes, J. Comp. Phys. 115 (1) (1994) 200–212. doi:10.1006/jcph.1994.1187.
URL http://www.sciencedirect.com/science/article/pii/S0021999184711879

[31] R. J. LeVeque, Finite Volume Methods for Hyperbolic Problems, Cambridge Texts in Applied Mathematics, 2002.

[32] E. F. Toro, R. C. Millington, L. A. M. Nejad, Godunov methods, Springer, 2001, Ch. Towards very high order Godunov schemes. doi:10.1007/978-1-4615-0663-8.

[33] E. F. Toro, V. A. Titarev, ADER schemes for scalar non-linear hyperbolic conservation laws with source terms in three-space dimensions, J. of Comp. Phys. 202 (1) (2005) 196–215. doi:10.1016/j.jcp.2004.06.014.
URL http://www.sciencedirect.com/science/article/pii/S0021999104002736

[34] M. Dumbser, C. D. Munz, ADER discontinuous Galerkin schemes for aeroacoustics, CR Acad. Sci. II B 333 (9) (2005) 683–687. doi:10.1016/j.crme.2005.07.008.
URL http://www.sciencedirect.com/science/article/pii/S1631072105001191

[35] V. Titarev, Derivative Riemann problem and ADER schemes, Ph.D. thesis, Università degli studi di Trento (2005).

[36] E. F. Toro, V. A. Titarev, TVD fluxes for the high-order ADER schemes, J. Sci. Comp. 24 (3) (2005) 285–309. doi:10.1007/s10915-004-4790-8.

[37] V. A. Titarev, E. F. Toro, ADER schemes for three-dimensional non-linear hyperbolic systems, J. Comp. Phys. 204 (2) (2005) 715–736. doi:10.1016/j.jcp.2004.10.028.
URL http://www.sciencedirect.com/science/article/pii/S0021999104004358

[38] E. F. Toro, M. Dumbser, V. A. Titarev, M. Käser, The derivative Riemann problem: the basis for high order ADER schemes, in: ECCOMAS CFD 2006: Proceedings of the European Conference on Computational Fluid Dynamics, Egmond aan Zee, The Netherlands, September 5-8, 2006, Delft University of Technology; European Community on Computational Methods in Applied Sciences (ECCOMAS), 2006.

[39] E. F. Toro, V. A. Titarev, Derivative Riemann solvers for systems of conservation laws and ADER methods, J. Comp. Phys. 212 (1) (2006) 150–165. doi:10.1016/j.jcp.2005.06.018.
URL http://www.sciencedirect.com/science/article/pii/S0021999105003141

[40] V. A. Titarev, E. F. Toro, ADER schemes for hyperbolic conservation laws with reactive terms, in: ECCOMAS CFD 2006: Proceedings of the European Conference on Computational Fluid Dynamics, Egmond aan Zee, The Netherlands, September 5-8, 2006, Delft University of Technology; European Community on Computational Methods in Applied Sciences (ECCOMAS), 2006.

[41] Y. Takakura, Direct-expansion forms of ADER schemes for conservation laws and their verification, J. Comp. Phys. 219 (2) (2006) 855–878. doi:10.1016/j.jcp.2006.05.013.

[42] V. A. Titarev, E. F. Toro, Analysis of ADER and ADER-WAF schemes, IMA J Num. Anal. 27 (3) (2007) 616–630. doi:10.1093/imanum/drl033.

[43] H. Zahran, Central ADER schemes for hyperbolic conservation laws, J. Math. Anal. Appl. 346 (1) (2008) 120–140. doi:10.1016/j.jmaa.2008.05.032.
URL http://www.sciencedirect.com/science/article/pii/S0022247X08005192

[44] M. Dumbser, D. S. Balsara, E. F. Toro, C.-D. Munz, A unified framework for the construction of one-step finite volume and discontinuous Galerkin schemes on unstructured meshes, J. Comput. Phys. 227 (18) (2008) 8209–8253. doi:https://doi.org/10.1016/j.jcp.2008.05.025.
URL http://www.sciencedirect.com/science/article/pii/S0021999108002829

[45] M. Dumbser, C. Enaux, E. F. Toro, Finite volume schemes of very high order of accuracy for stiff hyperbolic balance laws, J. Comput. Phys. 227 (8) (2008) 3971 – 4001. doi:https://doi.org/10.1016/j.jcp.2007.12.005.
URL http://www.sciencedirect.com/science/article/pii/S0021999107005578

[46] M. Dumbser, Arbitrary high order PNPM schemes on unstructured meshes for the compressible Navier-Stokes equations, Comput. Fluids 39 (1) (2010) 60–76. doi:10.1016/j.compfluid.2009.07.003.
URL http://www.sciencedirect.com/science/article/pii/S0045793009001030

[47] A. Hidalgo, M. Dumbser, ADER schemes for nonlinear systems of stiff advection–diffusion–reaction equations, J. Sci. Comput. 48 (1-3) (2011) 173–189. doi:10.1007/s10915-010-9426-6.

[48] W. Boscheri, M. Dumbser, A direct arbitrary-lagrangian-eulerian ADER-WENO finite volume scheme on unstructured tetrahedral meshes for conservative and non-conservative hyperbolic systems in 3D, J. Comput. Phys. 275 (2014) 484–523. doi:10.1016/j.jcp.2014.06.059.
URL http://www.sciencedirect.com/science/article/pii/S002199911400477X

[49] G. I. Montecinos, E. F. Toro, Reformulations for general advection–diffusion–reaction equations and locally implicit ADER schemes, J. Comput. Phys. 275 (2014) 415–442. doi:10.1016/j.jcp.2014.06.018.

[50] S. Busto, E. F. Toro, M. E. Vázquez-Cendón, Design and analisis of ADER–type schemes for model advection–diffusion–reaction equations, J. Comp. Phys. 327 (2016) 553–575. doi:10.1016/j.jcp.2016.09.043.

[51] A. Bermúdez, Continuum thermomechanics, Vol. 43 of Progress in Mathematical Physics, Birkhäuser Verlag, Basel, 2005.

[52] T. Chacón, R. Lewandowski, Mathematical and numerical foundations of turbulence models and applications, Modeling and simulation in science, engineering and technology, Birkhauser, 2014. doi:10.1007/978-1-4939-0455-6.

[53] V. V. Rusanov, The calculation of the interaction of non-stationary shock waves and obstacles, USSR Computational Mathematics and Mathematical Physics 1 (1962) 304–320.

[54] L. Cea, M. E. Vázquez-Cendón, Unstructured finite volume discretization of two-dimensional depth-averaged shallow water equations with porosity, Int. J. Numer. Methods Fluids 63 (8) (2010) 903–930. doi:10.1002/fld.2107.
URL http://onlinelibrary.wiley.com/doi/10.1002/fld.2107/full

[55] R. Bermejo, L. Saavedra, Modified Lagrange-Galerkin methods of first and second order in time for convection-diffusion problems, Numer. Math. 120 (2012) 601–638. doi:10.1007/s00211-011-0418-8.

[56] M. Schäfer, S. Turek, F. Durst, E. Krause, R. Rannacher, Benchmark Computations of Laminar Flow Around a Cylinder, Vieweg+Teubner Verlag, Wiesbaden, 1996, pp. 547–566. doi:10.1007/978-3-322-89849-4-39.
URL http://dx.doi.org/10.1007/978-3-322-89849-4-39

[57] J. Volker, Higher order finite element methods and multigrid solvers in a benchmark problem for the 3D Navier-Stokes equations, Int. J. Numer. Methods Fluids 40 (6) (2002) 775–798. doi:10.1002/fld.377.
URL http://dx.doi.org/10.1002/fld.377

Appendix A. LADER

ADER methodology was successfully extended in [50] to solve advection-diffusion-reaction equations. The developed method, ADER-ADRE, is of second order in space and time and stability can be ensured by determining the time step taking into account the advection, diffusion and reaction coefficients. Despite this method is easily programmed for the one dimensional code, the computation of the fluxes focusing on a particular finite volume at each time is not suitable for the mesh structure we have in the three-dimensional case. In this case, we would like to take profit from the loop on the faces of the finite volumes and reduce the computational cost. To do that, the LADER method, which preserves the second order and the stability of the ADER-ADRE method, was developed.

Let us consider the advection-diffusion-reaction equation

$$\partial_t q(x,t) + \lambda \partial_x q(x,t) = \partial_x \left(\alpha(x,t) \partial_x q(x,t) \right) + \beta q(x,t) \tag{A.1}$$

where

- $q(x,t)$ is the conservative variable,
- x, t are the spatial and temporal independent variables,
- λ is the characteristic speed,
- $\alpha(x,t)$ is the diffusion coefficient, a prescribed function,
- β is the coefficient of the reaction term.

Then, LADER method is divided into the following steps:

Step 1. Polynomial reconstruction. We consider a reconstruction of the data in terms of piecewise first-degree polynomials of the form

$$p_i(x) = \begin{cases} p_{i\,L}(x) = q_i^n + \Delta_{i\,L}^n (x - x_i), & x \in \left(x_{i-\frac{1}{2}}, x_i \right], \\ p_{i\,R}(x) = q_i^n + \Delta_{i\,R}^n (x - x_i), & x \in \left[x_i, x_{i+\frac{1}{2}} \right), \end{cases} \tag{A.2}$$

where $\Delta_{i\,L}^n$, $\Delta_{i\,R}^n$ denote the approximations of the spatial derivatives of $q(x,t)$ at time t^n related to two auxiliary elements of volume $\mathcal{C}_i = \left[x_{i-\frac{1}{2}}, x_{i+\frac{1}{2}} \right]$:

$$T_{i-1i\,L} = [x_i, x_{i+1}], \qquad T_{ii+1\,R} = [x_{i-1}, x_i] \tag{A.3}$$

(see Figure A.13).

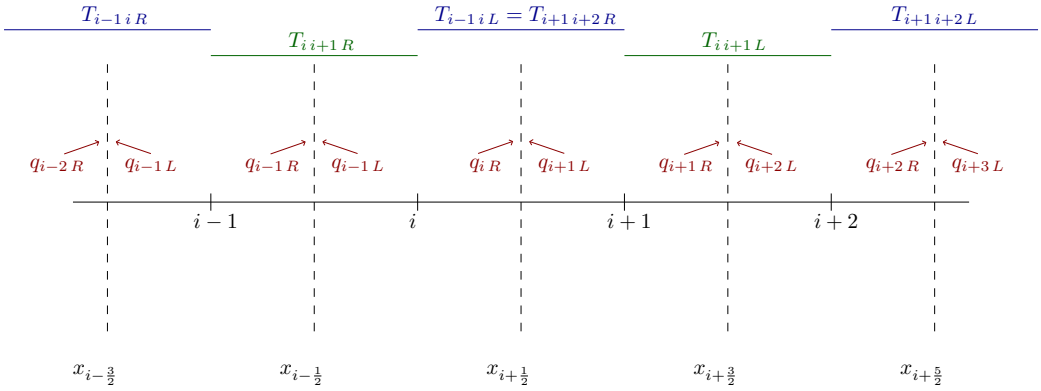

Figure A.13: Mesh and nomenclature.

Step 2. Solution of the generalized Riemann problem (GRP). To construct the numerical flux at $x_{i+\frac{1}{2}}$ the following generalizations of the Classical Riemann Problem are made. On the one hand, the initial condition is assumed to be a piecewise first-degree polynomial. On the other hand, the partial differential equation accounts for the diffusion and reaction terms. That leads to the problem

$$\begin{cases} \partial_t q\,(x,t) + \lambda \partial_x q\,(x,t) = \partial_x\left(\alpha \partial_x q\right)(x,t) + \beta q\,(x,t)\,, \\ q(x,0) = \begin{cases} p_{i\,R}(x), & x < 0, \\ p_{i+1\,L}(x), & x > 0. \end{cases} \end{cases} \tag{A.4}$$

Step 3. Diffusion and reaction terms. These terms are computed by approximating the integrals by the mid-point rule in both space and time.

The solution of the GRP at the interface $x_{i+\frac{1}{2}}$, set in Step 2, is expressed as a Taylor series expansion in time, namely,

$$\overline{q}_{i+\frac{1}{2}} = q(0,0_+) + \tau \partial_t q(0,0_+). \tag{A.5}$$

The first term of the above equation is computed as the solution of the classical Rieman problem

$$\begin{cases} \partial_t q\,(x,t) + \lambda \partial_x q\,(x,t) = 0, \\ q(x,0) = \begin{cases} q_{i\,R}, & x < 0, \\ q_{i+1\,L}, & x > 0, \end{cases} \end{cases} \tag{A.6}$$

where

$$q_{i\,R} = q_i + \frac{\Delta x}{2}\Delta^n_{i\,R} = q_i + \frac{q_i - q_{i-1}}{2} = \frac{1}{2}\left(3q_i - q_{i-1}\right), \tag{A.7}$$

$$q_{i+1\,L} = q_{i+1} - \Delta^n_{i+1\,L} = q_{i+1} - \frac{q_{i+2} - q_{i+1}}{2} = \frac{1}{2}\left(3q_{i+1} - q_{i+2}\right). \tag{A.8}$$

Then,

$$q\left(0, 0_+\right) = \begin{cases} q_{i\,R}, & \lambda > 0, \\ q_{i+1\,L}, & \lambda < 0. \end{cases}$$

The second term is computed following the Cauchy-Kovalevskaya procedure which allows us to express the time derivative of the conservative variable as a combination of the spatial derivatives,

$$\partial_t q(x,t) = -\lambda \partial_x q(x,t) + \partial_x\left(\alpha \partial_x q\right)(x,t) + \beta q\left(x,t\right), \tag{A.9}$$

so,

$$\overline{q}_{i+\frac{1}{2}} = q(0,0_+) + \tau\left[-\lambda \partial_x q(0,0_+) + \partial_x\left(\alpha \partial_x q\right)(0,0_+) + \beta q(0,0_+)\right]. \tag{A.10}$$

For now on, we will focus on the scheme for $\lambda > 0$ (the case $\lambda < 0$ is analogous). Approximating

$$\partial_x q(0,0_+) = \Delta^n_{i+\frac{1}{2}} \approx \frac{1}{\Delta x}\left(q^n_{i+1} - q^n_i\right), \tag{A.11}$$

$$\partial_x\left(\alpha \partial_x q\right)(0,0_+) = (\Delta \alpha \Delta)^n_{i+\frac{1}{2}}$$

$$\approx \frac{1}{\Delta x^2}\left[\alpha^n_{i+1}\left(q^n_{i+2} - q^n_{i+1}\right) - \alpha^n_i\left(q^n_i - q^n_{i-1}\right)\right] \tag{A.12}$$

and performing exact integration, the numerical flux reads

$$f^n_{i+\frac{1}{2}} = \lambda \overline{q}_{i-\frac{1}{2}^n} = \lambda\left\{q^n_{i\,R} + \frac{\Delta t}{2}\left[-\lambda \Delta^n_{i+\frac{1}{2}} + (\Delta \alpha \Delta)^n_{i+\frac{1}{2}} + \beta q^n_i\right]\right\}$$

$$= \lambda\left\{q^n_i + \frac{1}{2}\left(q^n_i - q^n_{i-1}\right) - \frac{\lambda \Delta t}{2\Delta x}\left(q^n_{i+1} - q^n_i\right)\right.$$

$$\left. + \frac{\Delta t}{2\Delta x^2}\left[\alpha^n_{i+1}\left(q^n_{i+2} - q^n_{i+1}\right) - \alpha^n_i\left(q^n_i - q^n_{i-1}\right)\right] + \beta \frac{\Delta t}{2} q^n_i\right\}. \tag{A.13}$$

For the diffusion and reaction terms computation we follow [50]. We consider the centred slopes

$$\Delta^n_i = \frac{q^n_{i+1} - q^n_{i-1}}{2\Delta x}, \tag{A.14}$$

$$(\Delta\alpha\Delta)_i^n = \frac{\alpha_{i+\frac{1}{2}}^n \left(q_{i+1}^n - q_i^n\right) - \alpha_{i-\frac{1}{2}}^n \left(q_i^n - q_{i-1}^n\right)}{\Delta x^2} \tag{A.15}$$

and the upwind slope

$$\breve{\Delta}_{i+\frac{1}{2}}^n = q_{i+1}^n - q_i^n. \tag{A.16}$$

Then, the evolved values of the diffusion and reaction terms read

$$\begin{aligned}\overline{(\Delta\alpha\Delta)_i^n} &= \frac{\overline{\alpha_{i+\frac{1}{2}}^n}\,\overline{\Delta_{i+\frac{1}{2}}} - \overline{\alpha_{i-\frac{1}{2}}^n}\,\overline{\Delta_{i-\frac{1}{2}}}}{\Delta x} = \frac{1}{\Delta x^2}\left(\overline{\alpha_{i+\frac{1}{2}}^n}\,\overline{\breve{\Delta}_{i+\frac{1}{2}}^n} - \overline{\alpha_{i-\frac{1}{2}}^n}\,\overline{\breve{\Delta}_{i-\frac{1}{2}}^n}\right) \\ &= \frac{1}{\Delta x^2}\left\{\left[\alpha_{i+\frac{1}{2}}^n + \frac{\Delta t}{2}\partial_t\alpha_{i+\frac{1}{2}}^n\right]\left[\breve{\Delta}_{i+\frac{1}{2}}^n + \frac{\Delta t}{2}\left((\Delta\alpha\Delta)_{i+1}^n - (\Delta\alpha\Delta)_i^n + \beta\breve{\Delta}_{i+\frac{1}{2}}^n\right)\right]\right. \\ &\left. + \left[\alpha_{i-\frac{1}{2}}^n + \frac{\Delta t}{2}\partial_t\alpha_{i-\frac{1}{2}}^n\right]\left[-\breve{\Delta}_{i-\frac{1}{2}}^n + \frac{\Delta t}{2}\left((\Delta\alpha\Delta)_{i-1}^n - (\Delta\alpha\Delta)_i^n - \beta\breve{\Delta}_{i-\frac{1}{2}}^n\right)\right]\right\},\end{aligned} \tag{A.17}$$

$$\beta\overline{q_i^n} = \beta\left[q_i^n + \frac{\Delta t}{2}\left(-\lambda\Delta_i^n + (\Delta\alpha\Delta)_i^n + \beta q_i^n\right)\right] \tag{A.18}$$

with $\overline{\alpha_{i+\frac{1}{2}}^n}$ and $\overline{\alpha_{i-\frac{1}{2}}^n}$ approximated likewise in [50].

Remark 2. *It is important to notice that the evolution of the diffusion term does not account for the advection term. The local treatment proposed in LADER scheme produce a evolved flux which already contains the whole contribution of the assembling of advection and diffusion terms. Hence, the second order of accuracy in space and time will be attained only if we neglect the advection term in the computation of the evolved diffusion.*

Finally, denoting $c = \frac{\lambda\Delta t}{\Delta x}$ the Courant number and $r = \beta\Delta t$ the reaction number, the finite volume scheme for the advection-diffusion-reaction equation results

$$\begin{aligned}q_i^{n+1} = q_i^n - c\left\{\breve{\Delta}_{i-\frac{1}{2}} + \frac{1}{2}\breve{\Delta}_{i-\frac{1}{2}}^n - \frac{c}{2}\breve{\Delta}_{i+\frac{1}{2}}^n + \frac{\Delta t}{2\Delta x^2}\left[\alpha_{i+1}^n\breve{\Delta}_{i+\frac{3}{2}}^n - \alpha_i^n\breve{\Delta}_{i-\frac{1}{2}}^n\right] + \frac{r}{2}\breve{\Delta}_{i-\frac{1}{2}}\right. \\ \left. - \frac{1}{2}\breve{\Delta}_{i-\frac{3}{2}}^n + \frac{c}{2}\breve{\Delta}_{i-\frac{1}{2}}^n - \frac{\Delta t}{2\Delta x^2}\left[\alpha_i^n\breve{\Delta}_{i+\frac{1}{2}}^n - \alpha_{i-1}^n\breve{\Delta}_{i-\frac{3}{2}}^n\right]\right\} + \frac{\Delta t}{\Delta x^2}\left\{\left[\alpha_{i+\frac{1}{2}}^n + \frac{\Delta t}{2}\partial_t\alpha_{i+\frac{1}{2}}^n\right]\right. \\ \left.\left[\breve{\Delta}_{i+\frac{1}{2}}^n + \frac{\Delta t}{2\Delta x^2}\left(\alpha_{i+\frac{3}{2}}^n\breve{\Delta}_{i+\frac{3}{2}}^n - 2\alpha_{i+\frac{1}{2}}^n\breve{\Delta}_{i+\frac{1}{2}}^n + \alpha_{i-\frac{1}{2}}^n\breve{\Delta}_{i-\frac{1}{2}}^n\right) + \frac{r}{2}\breve{\Delta}_{i+\frac{1}{2}}^n\right]\right.\end{aligned}$$

$$+\left[\alpha^n_{i-\frac{1}{2}}+\frac{\Delta t}{2}\partial_t\alpha^n_{i-\frac{1}{2}}\right]\left[-\breve{\Delta}^n_{i-\frac{1}{2}}+\frac{\Delta t}{2\Delta x^2}\left(-\alpha^n_{i+\frac{1}{2}}\breve{\Delta}^n_{i+\frac{1}{2}}+2\alpha^n_{i-\frac{1}{2}}\breve{\Delta}^n_{i-\frac{1}{2}}-\alpha^n_{i-\frac{3}{2}}\breve{\Delta}^n_{i-\frac{3}{2}}\right)\right.$$
$$\left.-\frac{r}{2}\breve{\Delta}^n_{i-\frac{3}{2}}\right]\Bigg\}+r\left[q^n_i-\frac{c}{4}\left(q^n_{i+1}-q^n_{i-1}\right)+\frac{\Delta t}{2\Delta x^2}\left(\alpha^n_{i+\frac{1}{2}}\breve{\Delta}^n_{i+\frac{1}{2}}-\alpha^n_{i-\frac{1}{2}}\breve{\Delta}^n_{i-\frac{1}{2}}\right)+\frac{r}{2}q^n_i\right]. \tag{A.19}$$

Remark 3. *The scheme for the advection-diffusion-reaction equation with constant diffusion coefficient reads*

$$\begin{aligned}q^{n+1}_i=q^n_i&-c\left[\breve{\Delta}^n_{i-\frac{1}{2}}+\frac{1}{2}\breve{\Delta}^n_{i-1}-\frac{c}{2}\breve{\Delta}^n_i+\frac{d}{2}\left(\breve{\Delta}^n_{i+1}-\breve{\Delta}^n_{i-1}\right)+\frac{r}{2}\breve{\Delta}^n_{i-\frac{1}{2}}\right]\\&+d\left[\breve{\Delta}^n_i+\frac{d}{2}\left(\breve{\Delta}^n_{i+1}-2\breve{\Delta}^n_i+\breve{\Delta}^n_{i-1}\right)+\frac{r}{2}\breve{\Delta}^n_i\right]\\&+r\left[q^n_i-\frac{c}{4}\left(q^n_{i+1}-q^n_{i-1}\right)+\frac{d}{2}\breve{\Delta}^n_i+\frac{r}{2}q^n_i\right]\end{aligned} \tag{A.20}$$

where $d=\frac{\alpha\Delta t}{\Delta x^2}$ *and* $\breve{\Delta}^n_i=q^n_{i+1}-2q^n_i+q^n_{i-1}$.

Remark 4. *There exist* c_M, d_M, $r_m\in\mathbb{R}$ *such that the LADER scheme,* (A.20)*, is stable in the 4-orthotopes*

$$\begin{aligned}O_{c_M,d_M,r_m}=\{(\theta,c,r,d)\mid\theta\in[-\pi,\pi],\ c\in[0,c_M],\ d\in[0,d_M],\\ r\in[r_m,0],\ c_M,\ d_M\in\mathbb{R}^+,\ r_m\in\mathbb{R}^-\}.\end{aligned} \tag{A.21}$$

To represent a feasible 4-orthotope we consider the isosurface of level one of

$$m_\theta(c,d,r)=\max_{\theta\in[-\pi,\pi]}\|A(\theta,c,d,r)\| \tag{A.22}$$

where $A(\theta,c,d,r)$ *is the function of the amplification factor of the scheme (see [50]). In Figure A.14 we can observe that the 4-orthotope defined by* $c_M=0.3$, $d_M=0.2$ *and* $r_m=-0.5$ *is embedded in the stability region.*

Lemma 1. *LADER scheme,* (A.19)*, is of second order in time and space.*

Proof. To prove the accuracy of Scheme (A.19), we recall the analysis carried out for the ADER scheme introduced in [50] and we detail the terms which have changed:

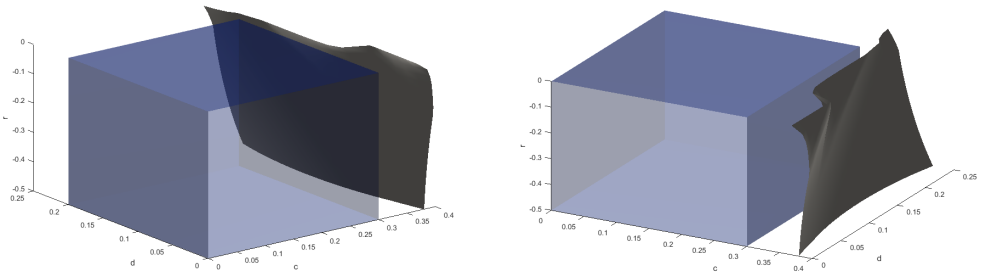

Figure A.14: Two different views of the isosurface of level one of function m_θ, (A.22), (grey) and the 4-orthotope of stability $\mathcal{O}_{0.3,0.2,-0.5}$ for the linear advection-diffusion-reaction equation (blue).

- Local truncation error contribution of the flux term neglecting the diffusion term contribution:

$$
\begin{aligned}
& \frac{\lambda}{\Delta x}\left[q(x_i,t^n)-(x_{i-1},t^n)+\frac{1}{2}\left(q(x_i,t^n)-2q(x_{i-1},t^n)+q(x_{i-2},t^n)\right)\right. \\
& \left.-\frac{c}{2}\left(q(x_{i+1},t^n)-2q(x_i,t^n)+q(x_{i-1},t^n)\right)\right] \\
= \quad & \frac{\lambda}{\Delta x}\left\{\partial_x q(x_i,t^n)\Delta x-\frac{1}{2}\partial_x^{(2)}q(x_i,t^n)\Delta x^2+\frac{1}{6}\partial_x^{(3)}q(x_i,t^n)\Delta x^3+\mathcal{O}\left(\Delta x^4\right)\right. \\
& +\frac{1}{2}\left[\partial_x^{(2)}q(x_i,t^n)\Delta x^2-\partial_x^{(3)}q(x_i,t^n)\Delta x^3+\mathcal{O}\left(\Delta x^4\right)\right] \\
& \left.-\frac{c}{2}\left[\partial_x^{(2)}q(x_i,t^n)\Delta x^2-\frac{1}{12}\partial_x^{(4)}q(x_i,t^n)\Delta x^4+\mathcal{O}\left(\Delta x^5\right)\right]\right\} \\
= \quad & \lambda\partial_x q(x_i,t^n)-\frac{\lambda^2\Delta t}{2}\partial_x^{(2)}q(x_i,t^n)+\mathcal{O}\left(\Delta x^2\right) \qquad \text{(A.23)}
\end{aligned}
$$

- Local truncation error contribution of the diffusion term to the flux term:

$$
\begin{aligned}
& \frac{\lambda\Delta t}{2\Delta x^2}\left\{\left[\alpha(x_{i+1},t^n)\frac{q(x_{i+2},t^n)-q(x_{i+1},t^n)}{\Delta x}-\alpha(x_i,t^n)\frac{q(x_i,t^n)-q(x_{i-1},t^n)}{\Delta x}\right]\right. \\
& \left.-\left[\alpha(x_i,t^n)\frac{q(x_{i+1},t^n)-q(x_i,t^n)}{\Delta x}-\alpha(x_{i-1},t^n)\frac{q(x_{i-1},t^n)-q(x_{i-2},t^n)}{\Delta x}\right]\right\}
\end{aligned}
$$

$$
\begin{aligned}
= \quad & \frac{\lambda\Delta t}{2\Delta x^3}\left\{\alpha(x_{i+1},t^n)\left[\partial_x q(x_i,t^n)\Delta x+\frac{3}{2}\partial_x^{(2)}q(x_i,t^n)\Delta x^2\right.\right.\\
& +\left.\frac{7}{6}\partial_x^{(3)}q(x_i,t^n)\Delta x^3+\mathcal{O}(\Delta x^4)\right]-\alpha(x_i,t^n)\left[\right.\\
& \left.\left.2\partial_x q(x_i,t^n)\Delta x+\frac{1}{3}\partial_x^{(3)}q(x_i,t^n)\Delta x^3+\mathcal{O}(\Delta x^4)\right)\right]\\
& +\alpha(x_{i-1},t^n)\left[\partial_x q(x_i,t^n)\Delta x-\frac{3}{2}\partial^{(2)}q(x_i,t^n)\Delta x^2\right.\\
& \left.+\frac{7}{6}\partial^{(3)}q(x_i,t^n)\Delta x^3+\mathcal{O}(\Delta x^4)\right]\\
= \quad & \frac{\lambda\Delta t}{2\Delta x^3}\left[\partial_x^{(2)}\alpha(x_i,t^n)\partial_x q(x_i,t^n)\Delta x^3+3\partial_x\alpha_i^n\partial_x^{(2)}q(x_i,t^n)\Delta x^3\right.\\
& \left.+2\alpha_i^n\partial_x^{(3)}q(x_i,t^n)\Delta x^3+\mathcal{O}\left(\Delta x^4\right)\right]\\
= \quad & \frac{\lambda\Delta t}{2}\left[\partial_x^{(2)}\left(\alpha(x_i,t^n)\partial_x q(x_i,t^n)\right)+\partial_x\left(\alpha(x_i,t^n)\partial_x^{(2)}q(x_i,t^n)\right)\right]\\
& +\mathcal{O}(\Delta x\Delta t)
\end{aligned}
\tag{A.24}
$$

854 • Local truncation error contribution of the diffusion term:

$$
\begin{aligned}
& -\frac{1}{\Delta x^2}\left\{\overline{\alpha}(x_{i+\frac{1}{2}},t^n)\left[q(x_{i+1},t^n)-q(x_i,t^n)\right.\right.\\
& +\left.+\frac{\Delta t}{2}\left(\frac{1}{\Delta x^2}\alpha(x_{i+\frac{3}{2}},t^n)\left[q(x_{i+2},t^n)-q(x_{i+1},t^n)\right]\right.\right.\\
& -\left.\frac{1}{\Delta x^2}\alpha(x_{i+\frac{1}{2}},t^n)\left[2q(x_{i+1},t^n)-2q(x_i,t^n)\right]\right.\\
& +\left.\frac{1}{\Delta x^2}\alpha(x_{i-\frac{1}{2}},t^n)\left[q(x_i,t^n)-q(x_{i-1},t^n)\right]\right.\\
& \left.\left.+\left.\beta\left[q(x_{i+1},t^n)-q(x_i,t^n)\right]\right)\right]\\
& +\overline{\alpha}(x_{i-\frac{1}{2}},t^n)\left[\right.\left.q(x_{i-1},t^n)-q(x_i,t^n)\right.\\
& +\left.\frac{\Delta t}{2}\left(-\frac{1}{\Delta x^2}\alpha(x_{i+\frac{1}{2}},t^n)\left[q(x_{i+1},t^n)-q(x_i,t^n)\right]\right.\right.\\
& +\left.\left.\frac{1}{\Delta x^2}\alpha(x_{i-\frac{1}{2}},t^n)\left[2q(x_i,t^n)-2q(x_{i-1},t^n)\right]\right.\right.
\end{aligned}
$$

$$
\begin{aligned}
& - \frac{1}{\Delta x^2}\alpha(x_{i-\frac{3}{2}},t^n)\left[q(x_{i-1},t^n)-q(x_{i-2},t^n)\right] \\
& + \beta\left[q(x_{i-1},t^n)-q(x_i,t^n)\right]\Big)\Big]\Big\} \\
= \quad & -\partial_x\left(\alpha(x_i,t^n)\partial_x q(x_i,t^n)\right)+\frac{\Delta t}{2}\Big\{\partial_x\left(\partial_t\alpha(x_i,t^n)\partial_x q(x_i,t^n)\right) \\
& +\partial_x\left[\alpha(x_i,t^n)\partial_x^{(2)}\left(\alpha(x_i,t^n)\partial_x q(x_i,t^n)\right)\right] \\
& +\beta\partial_x\left(\alpha(x_i,t^n)\partial_x q(x_i,t^n)\right)\Big\}+\mathcal{O}(\Delta x^2)+\mathcal{O}(\Delta x\Delta t). \qquad \text{(A.25)}
\end{aligned}
$$

Finally, taking into account the truncation error of the remaining terms of the scheme and Cauchy-Kovalevskaya equality, we get

$$
\begin{aligned}
\tau^n = \quad & \partial_t q(x_i,t^n)+\lambda\partial_x q(x_i,t^n)-\partial_x\left[\alpha(x_i,t^n)\partial_x q(x_i,t^n)\right]-\beta q(x_i,t^n) \\
& +\frac{\Delta t}{2}\Big\{\partial_t^{(2)}q(x_i,t^n)+\lambda\partial_x\left[-\lambda\partial_x q(x_i,t^n)+\beta q(x_i,t^n)\right] \\
& -\beta\left[-\lambda\partial_x q(x_i,t^n)+\beta q(x_i,t^n)\right]-\partial_x\left[\partial_t\alpha(x_i,t^n)\partial_x q(x_i,t^n)\right] \\
& +\lambda\partial_x\left[\alpha(x_i,t^n)\partial_x^{(2)}q(x_i,t^n)\right]-\partial_x\left\{\alpha(x_i,t^n)\partial_x^{(2)}\left[\alpha(x_i,t^n)\partial_x q(x_i,t^n)\right]\right\} \\
& -\beta\partial_x\left[\alpha(x_i,t^n)\partial_x q(x_i,t^n)\right]-\beta\partial_x\left[\alpha(x_i,t^n)\partial_x q(x_i,t^n)\right] \\
& +\partial_x^{(2)}\left[\alpha(x_i,t^n)\partial_x q(x_i,t^n)\right]\Big\}+\mathcal{O}\left(\Delta t^2\right)+\mathcal{O}\left(\Delta x^2\right)+\mathcal{O}\left(\Delta x\Delta t\right) \\
= \quad & \mathcal{O}\left(\Delta t^2\right)+\mathcal{O}\left(\Delta x^2\right)+\mathcal{O}(\Delta x\Delta t). \qquad \text{(A.26)}
\end{aligned}
$$

□

Appendix B. Manufactured tests. Source terms

In this appendix we describe the source terms used in the manufactured test (see Sections 4.1 and 4.2):

- Manufactured test 1. Laminar flow.

$$
\begin{aligned}
\mathbf{f}_{\mathbf{u}_1}(x,y,z,t) = \quad & \pi y\cos(\pi ty)\cos(\pi tz)-\pi t\sin(\pi t(x+y+z)) \\
& -\pi z\sin(\pi ty)\sin(\pi tz)+2\pi^2t^2\mu\sin(\pi ty)\cos(\pi tz) \\
& -\pi t\cos(\pi tz^3)\cos(\pi ty)\cos(\pi tz) \\
& -\pi t\sin(\pi ty)\sin(\pi tz)\exp(-2\pi t^2x), \qquad \text{(B.1)}
\end{aligned}
$$

$$\begin{aligned}
\mathbf{f}_{\mathbf{u}_2}(x,y,z,t) &= \pi z^3\sin(\pi t z^3) - \pi t\sin(\pi t(x+y+z)) - 6\pi t z\mu\sin(\pi t z^3)\\
&\quad -9\pi^2 t^2 z^4\mu\cos(\pi t z^3) + 3\pi t z^2\exp(-2\pi t^2 x)\sin(\pi t z^3), \qquad \text{(B.2)}\\
\mathbf{f}_{\mathbf{u}_3}(x,y,z,t) &= -\pi t\sin(\pi t(x+y+z)) - 4\pi^2 t^4\mu\exp(-2\pi t^2 x)\\
&\quad -4\pi t x\exp(-2\pi t^2 x)\\
&\quad -2\pi t^2\sin(\pi t y)\exp(-2\pi t^2 x)\cos(\pi t z). \qquad \text{(B.3)}
\end{aligned}$$

862 • Manufactured test 2. Turbulent flow with species transport.

$$\begin{aligned}
\mathbf{f}_{\mathbf{u}_1}(x,y,z,t) &= (2\pi t\cos(\pi t x))/3 - \pi t\sin(\pi t(x+y+z)) + \pi y\cos(\pi t y)\cos(\pi t z)\\
&\quad -\pi z\sin(\pi t y)\sin(\pi t z) + 2\pi^2 t^2\mu\sin(\pi t y)\cos(\pi t z)\\
&\quad -\pi t\cos(\pi t z^3)\cos(\pi t y)\cos(\pi t z) - \pi t\sin(\pi t y)\sin(\pi t z)\exp(-2\pi t^2 x)\\
&\quad +(2\pi^2 C_\mu t^2\sin(\pi t y)\cos(\pi t z)(\sin(\pi t x)+2)^2)/(\exp(-\pi t z)+1)\\
&\quad +(\pi^2 C_\mu t^2\sin(\pi t y)\sin(\pi t z)\exp(-\pi t z)\\
&\quad (\sin(\pi t x)+2)^2)/(\exp(-\pi t z)+1)^2, \qquad \text{(B.4)}\\
\mathbf{f}_{\mathbf{u}_2}(x,y,z,t) &= \pi z^3\sin(\pi t z^3) - \pi t\sin(\pi t(x+y+z)) - 6\pi t z\mu\sin(\pi t z^3)\\
&\quad 9\pi^2 t^2 z^4\mu\cos(\pi t z^3) + 3\pi t z^2\exp(-2\pi t^2 x)\sin(\pi t z^3)\\
&\quad -(9\pi^2 C_\mu t^2 z^4\cos(\pi t z^3)(\sin(\pi t x)+2)^2)/(\exp(-\pi t z)+1)\\
&\quad -(6\pi C_\mu t z\sin(\pi t z^3)(\sin(\pi t x)+2)^2)/(\exp(-\pi t z)+1)\\
&\quad -(3\pi^2 C_\mu t^2 z^2\exp(-\pi t z)\sin(\pi t z^3)\\
&\quad (\sin(\pi t x)+2)^2)/(\exp(-\pi t z)+1)^2, \qquad \text{(B.5)}\\
\mathbf{f}_{\mathbf{u}_3}(x,y,z,t) &= (4\pi^2 C_\mu t^3\exp(-2\pi t^2 x)\cos(\pi t x)(\sin(\pi t x)+2))/(\exp(-\pi t z)+1)\\
&\quad -4\pi^2 t^4\mu\exp(-2\pi t^2 x) - 4\pi t x\exp(-2\pi t^2 x)\\
&\quad -2\pi t^2\sin(\pi t y)\exp(-2\pi t^2 x)\cos(\pi t z)\\
&\quad -(4\pi^2 C_\mu t^4\exp(-2\pi t^2 x)(\sin(\pi t x)+2)^2)/(\exp(-\pi t z)+1)\\
&\quad -\pi t\sin(\pi t(x+y+z)), \qquad \text{(B.6)}\\
f_k(x,y,z,t) &= \exp(-\pi t z) + \pi x\cos(\pi t x)\\
&\quad -(C_\mu(\sin(\pi t x)+2)^2(2\pi t^2\exp(-2\pi t^2 x)\\
&\quad +\pi t\sin(\pi t y)\sin(\pi t z))^2)/(\exp(-\pi t z)+1)\\
&\quad +\pi^2 t^2\mu\sin(\pi t x) + \pi t\sin(\pi t y)\cos(\pi t x)\cos(\pi t z)\\
&\quad -(9\pi^2 C_\mu t^2 z^4\sin(\pi t z^3)^2(\sin(\pi t x)+2)^2)/(\exp(-\pi t z)+1)\\
&\quad -(\pi^2 C_\mu t^2\cos(\pi t y)^2\cos(\pi t z)^2(\sin(\pi t x)+2)^2)/(\exp(-\pi t z)+1)\\
&\quad -(2\pi^2 C_\mu t^2\cos(\pi t x)^2(\sin(\pi t x)+2))/(\sigma_k(\exp(-\pi t z)+1))\\
&\quad +(\pi^2 C_\mu t^2\sin(\pi t x)(\sin(\pi t x)+2)^2)/(\sigma_k(\exp(-\pi t z)+1)) + 1, \qquad \text{(B.7)}\\
f_\varepsilon(x,y,z,t) &= (C_{2\,\varepsilon}(\exp(-\pi t z)+1)^2)/(\sin(\pi t x)+2) - \pi z\exp(-\pi t z)\\
&\quad -\pi^2 t^2\mu\exp(-\pi t z)
\end{aligned}$$

$$
\begin{aligned}
& -(C_{1\,\varepsilon}(\exp(-\pi tz)+1)((C_\mu(\sin(\pi tx)+2)^2(2\pi t^2\exp(-2\pi t^2x) \\
& +\pi t\sin(\pi ty)\sin(\pi tz))^2)/(\exp(-\pi tz)+1) \\
& +(9\pi^2C_\mu t^2z^4\sin(\pi tz^3)^2(\sin(\pi tx)+2)^2)/(\exp(-\pi tz)+1) \\
& +(\pi^2C_\mu t^2\cos(\pi ty)^2\cos(\pi tz)^2(\sin(\pi tx) \\
& +2)^2)/(\exp(-\pi tz)+1)))/(\sin(\pi tx)+2) \\
& -\pi t\exp(-\pi tz)\exp(-2\pi t^2x) \\
& -(\pi^2C_\mu t^2\exp(-\pi tz)(\sin(\pi tx)+2)^2)/(\sigma_\varepsilon(\exp(-\pi tz)+1)) \\
& +(\pi^2C_\mu t^2\exp(-2\pi tz)(\sin(\pi tx)+2)^2)/(\sigma_\varepsilon(\exp(-\pi tz)+1)^2), \qquad \text{(B.8)}
\end{aligned}
$$

$$
\begin{aligned}
f_y(x,y,z,t) \quad = \quad & \pi x\cos(\pi tx)+\pi^2t^2\sin(\pi tx)(\mathcal{D}+(C_\mu(\sin(\pi tx) \\
& +2)^2)/(Sc_t(\exp(-\pi tz)+1))) \\
& +\pi t\sin(\pi ty)\cos(\pi tx)\cos(\pi tz) \\
& -(2\pi^2C_\mu t^2\cos(\pi tx)^2(\sin(\pi tx)+2))/(Sc_t(\exp(-\pi tz)+1)). \qquad \text{(B.9)}
\end{aligned}
$$

863